ANDRA BGR CHEVRON CRIEPI DOE ENRESA ENSI GRS IRSN
JAEA NAGRA NWMO OBAYASHI SCK•CEN SWISSTOPO

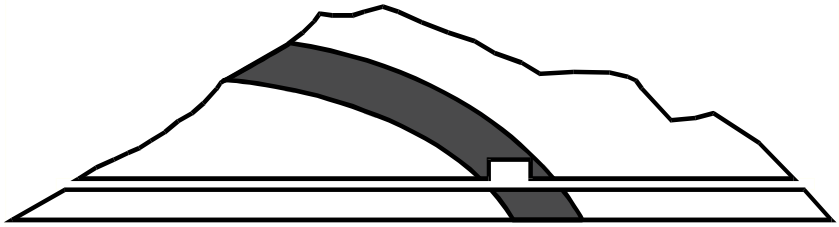

Mont Terri Project

TECHNICAL NOTE 2015-43

April 2015

HE-E Experiment: Laboratory test in a THM cell with the Sand/Bentonite mixture

M.V. Villar, P.L. Martín, F.J. Romero, R. Gómez-Espina, R.J. Iglesias, V. Gutiérrez-Rodrigo

CIEMAT, Madrid, Spain

Distribution:

Standard distribution:

ANDRA (S. Dewonck)

BGR (K. Schuster)

CHEVRON (P. Connolly)

CRIEPI (T. Oyama)

DOE (P.Nair, J. Birkholzer)

ENRESA (J.C. Mayor)

ENSI (E. Frank)

GRS (K. Wieczorek)

IRSN (J.-M. Matray)

JAEA (N. Shigeta)

NAGRA (T. Vietor)

NWMO (M. Jensen)

OBAYASHI (H. Kawamura, T. Kikuchi)

SCK•CEN (C. Bruggeman)

SWISSTOPO (P. Bossart, A. Möri and Ch. Nussbaum)

Additional distribution:

NAGRA (I. Gaus, T. Sakaki)

UPC (A. Gens)

Every organisation & contractor takes care of their own distribution.

Contents

Acknowledgements

The research leading to these results received funding until February 2014 from the European Atomic Energy Community's Seventh Framework Programme (FP7/2007-2011) under Grant Agreement n°249681 (PEBS project) and from ENRESA through a CIEMAT-ENRESA General Agreement. From March 2014 it has been financed by the Mont Terri Consortium. The tests reported here were carried out at CIEMAT's facilities with the help of Ramón Campos and Juan Aroz. The data acquisition system was developed by José Miguel Barcala. The pore size distribution measurements were done by A.M. González and R. Campos in the Laboratory of Petrophysics led by Dr. Rocío Campos.

1 Introduction

A common design of a high-level radioactive waste (HLW) disposal system consists of the wastes encapsulated within steel canisters that are emplaced within horizontal tunnels, with the space between the canisters and the surrounding rock filled with a bentonite-based material. In the early post closure period the buffer is expected to experience the maximum temperature. In this phase the buffer is largely unsaturated and the thermal evolution of the engineered barrier system (EBS) is likely to be controlled by the effective thermal conductivity of the dry buffer.

In particular, the temperature evolution of the EBS and surrounding host rock was simulated using reference data for the thermal properties of HLW, bentonite backfill and Opalinus Clay. The results showed that the canister surface temperatures would reach a maximum value of ~150°C within a few years after emplacement (Johnson *et al*. 2002). These anticipated temperatures at the canister surface, in the bentonite and at the bentonite-host rock interface were scaled down in time and space to meet the specifications of the HE-E experiment, which started in the framework of PEBS (Gaus *et al*. 2011). The HE-E experiment targets the period immediately after repository closure when the temperatures are maximal and the moisture content is low but increasing.

The HE-E experiment is a 1:2 scale heating experiment considering natural resaturation of the EBS and a maximum heater surface temperature of 140°C. Heater temperature increased almost linearly to its maximum value in a period of one year after which the temperature was held constant. The experiment is located at the Mont Terri URL (Switzerland) in a 50-m long non-lined horizontal microtunnel of 1.3 m diameter excavated in 1999 in the shaly facies of the Opalinus Clay. The test section of the microtunnel was characterised in detail during the Ventilation Experiment (ENRESA 2005). The detailed design of the experiment is described in Teodori & Gaus (2011).

The experiment consists of two independently heated sections (Figure 1), where the heaters are placed in a steel liner supported by MX80 bentonite blocks (dry density 1.81 g/cm^3, water content 10.3%). The two sections are fully symmetric apart from the granular material filling the rest of the gallery: whereas section 1 is filled with pure MX80 bentonite pellets, section 2 is filled with a 65/35 granular sand/bentonite mixture. The characteristics of both materials are described below:

- The granular bentonite (B) has been adopted in the Swiss disposal concept. It is the same as the one used for the ESDRED project, mixture type E (sodium bentonite MX-80 from Wyoming). The material was described in detail in Plötze & Weber (2007). Once emplaced its water content was 5.9% and the dry average density was 1.46 kg/m^3.
- The sand/bentonite (S/B) mixture (having a higher thermal conductivity) was selected by GRS and provided by MPC (Limay, France). The components were 65 % of quartz sand with a grain spectrum of 0.5 – 1.8 mm and 35 % of sodium bentonite GELCLAY WH2 (granular material of the same composition as MX-80) of the same grain spectrum, which was obtained by crushing and sieving from the qualified raw material. Water content was 13% for the bentonite and 0.05% for the sand, giving an average water content of the mixture in the range of 4%. There is some uncertainty about the actual emplaced density of the mixture, and values as low as 1.26 g/cm^3 have been given. However, based on the tests performed to check the emplacement technique, an average value of 1.5 g/cm^3 was taken.

A heater system, capable of representing the temperature curve of the anticipated heat production in the canisters (up to a maximum of 140°C), was switched on June the 28th, 2011. During the experiment the temperature, humidity and the water saturation are monitored through a system of sensors on the heater surface within the liner, in the bentonite and in the surrounding host rock.

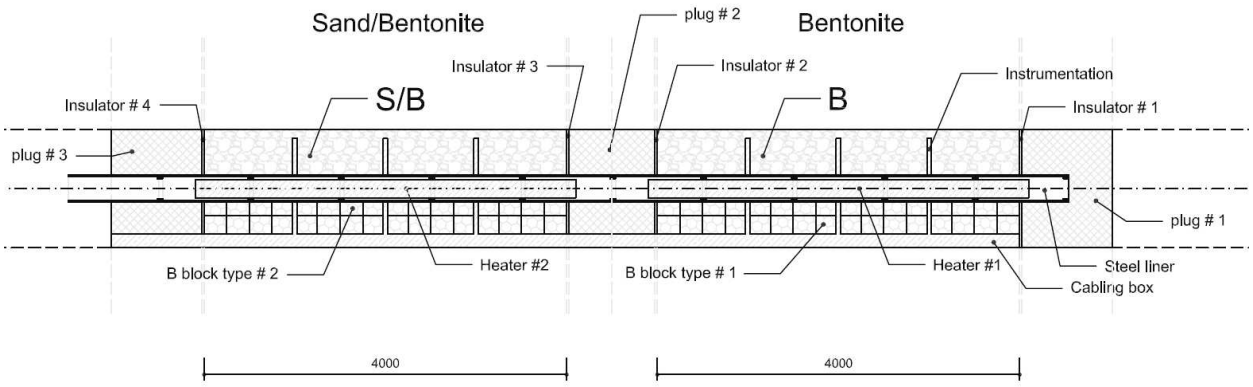

Figure 1: Layout of the *in situ* HE-E experiment

The performance of tests at different scales, in both the laboratory and the field, is very useful to observe the thermo-hydro-mechanical processes taking place in the engineered barriers and the geological medium. They also provide the information required for the verification and validation of mathematical models of the coupled processes and their numerical implementation. The laboratory tests in cells are particularly helpful to identify and quantify processes in a shorter period of time and with less uncertainty regarding the boundary conditions than the *in situ* tests. In the tests in cells the sealing material is subjected simultaneously to heating and hydration in opposite directions, in order to simulate the conditions of the clay barrier in the repository, i.e. the interaction of the water coming from the host rock and the thermal gradient generated by the heat emitted by the wastes in the canisters. With the aim of complementing the information provided by the HE-E *in situ* test, CIEMAT undertook, in the framework of the PEBS project, the performance of two tests in cells simulating the conditions of the sealing materials used in the two sections of the *in situ* test. From the end of the PEBS project (February 2014), the laboratory tests went on under contract with the Mont Terri consortium.

The cell with the S/B material was dismantled in February 2015, after more than three years of operation. This report refers to the results obtained in cell S/B during operation and to the postmortem analyses of the material. The results obtained until the end of the PEBS project were given in Villar et al. 2012 and 2014. The details given in these reports are not given again here, but just summarised.

2 Material

The material used in the laboratory test is the same as that used in the *in situ* test and was sent to CIEMAT directly from the Mont Terri test site. A plastic bucket with 25 kg of the sand/bentonite mixture (S/B) was received at CIEMAT on April 2011 (Figure 2). The as-received water content of the material was 3.6%. The granulometric curve obtained by dry sieving in our laboratory is shown in Figure 3.

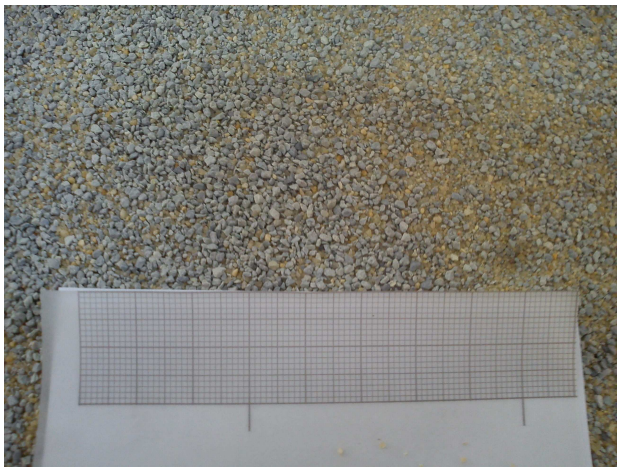

Figure 2: Appearance of the sand/bentonite mixture received at CIEMAT

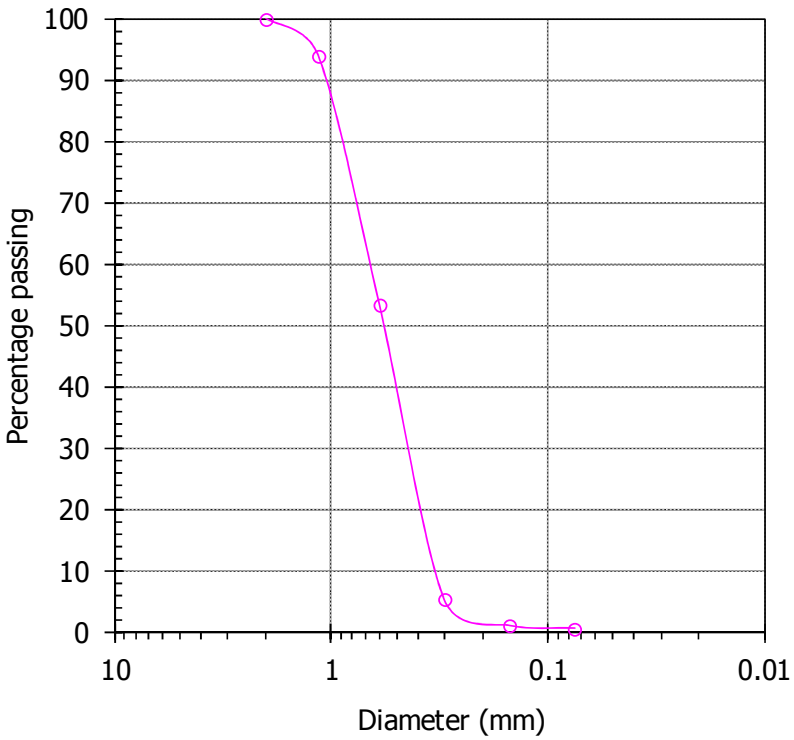

Figure 3: Granulometric curve obtained by dry sieving of the material used in the tests

The dry density of the solid grains determined with pycnometers using water as dispersing agent was 2.71 g/cm^3; the external specific surface area determined by the 9-point BET method was 5 m^2/g; and the superficial thermal conductivity in the as-received state determined at room temperature using the transient hot wire method (KEMTHERM QTM-D3) was 0.33 W/m·K. The specific heat capacity of the material ground and dried at 110°C was determined in a TG-DSC Setsys Evolution 16 equipment. The determination was performed in the range of temperatures from 22 to 298°C. The values obtained ranged between 0.74 J/g·K (at 22°C) and 0.90 J/g·K (at 115°C) (Fernández 2011). The pore size distribution of the uncompacted material was obtained by mercury intrusion porosimetry. The S/B mixture has a predominant macroporosity with a pore mode about 204 µm (Villar 2013).

The swelling pressure of the sand/bentonite mixture was determined in standard oedometers in samples initially compacted at a nominal dry density of 1.45 g/cm^3. An average swelling

pressure of 1.5 MPa was obtained for the samples saturated with deionised water and of 0.7 MPa for the samples saturated with Pearson water, which is a sodium-chloride water with a salinity of 19 g/L reproducing the host rock pore water (Pearson 1998). Its chemical composition is indicated in Table 1.

Table 1: Chemical composition of the water used in the tests (mg/L)

Cl^-	SO_4^{2-}	HCO_3^-	Mg^{2+}	Ca^{2+}	Na^+	K^+	Sr^+	pH
10636	1354	26	413	1034	5550	63	47	7.6

3 Experimental setup

In the tests in cells a column of material is hydrated through the upper surface whereas the lower surface is heated at a constant temperature. The infiltration test for the HE-E was performed in a cylindrical cell similar to the cells already used during the FEBEX and NF-PRO projects (Villar *et al*. 2005a, b, 2008). The nominal internal diameter of the cell was 7 cm and inner length 50 cm, therefore, those were the dimensions of the sample column (Figure 4). The body of the cells consisted of four cylindrical elements made of Teflon PTFE (thermal conductivity 0.25 W/m·K) to prevent as much as possible lateral heat conduction. The cell was wrapped with insulation wool to avoid the heat loss.

The bottom part of the cell had a plane stainless steel heater, and the power supplied to the resistance was measured online. Inside the upper steel plug of the cells there was a deposit in which water circulated at room temperature. In this way, a constant temperature gradient between top and bottom of the sample was imposed. Hydration took place through the upper lid of the cell. Pearson water was supplied from a deposit hanging from an electronic load cell, and the water intake was measured by changes in the weight of the deposit. Since the water availability at the Mont Terri gallery is very limited, only a small pressure, given by an equivalent 60-cm high water column, was applied to the saturation water.

The walls of the cell were perforated for the installation of capacitive-type sensors placed in the axis of the column at three different levels (10, 22 and 40 cm from the heater approximately). The transducers used were VAISALA HMT334 protected by cylindrical stainless steel filters. The accuracy of the humidity sensor was ±1% over the range 0-90 percent RH and ±2% over the range 90-100 percent RH.

The water volume intake, the heater power and the relative humidity (RH) and temperature (*T*) at different levels inside the clay were measured as a function of time. A schematic diagram of the setup is shown in Figure 5. The different components of the system were described in detail in Villar et al. (2012).

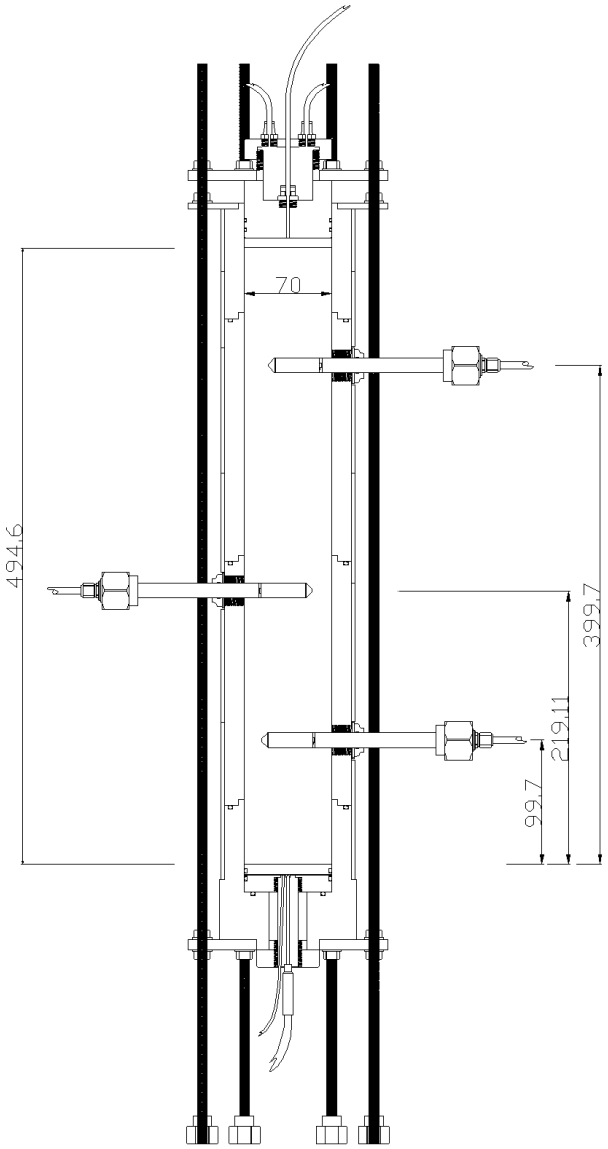

Figure 4: Schematic design of the cell and sensors (dimensions in mm)

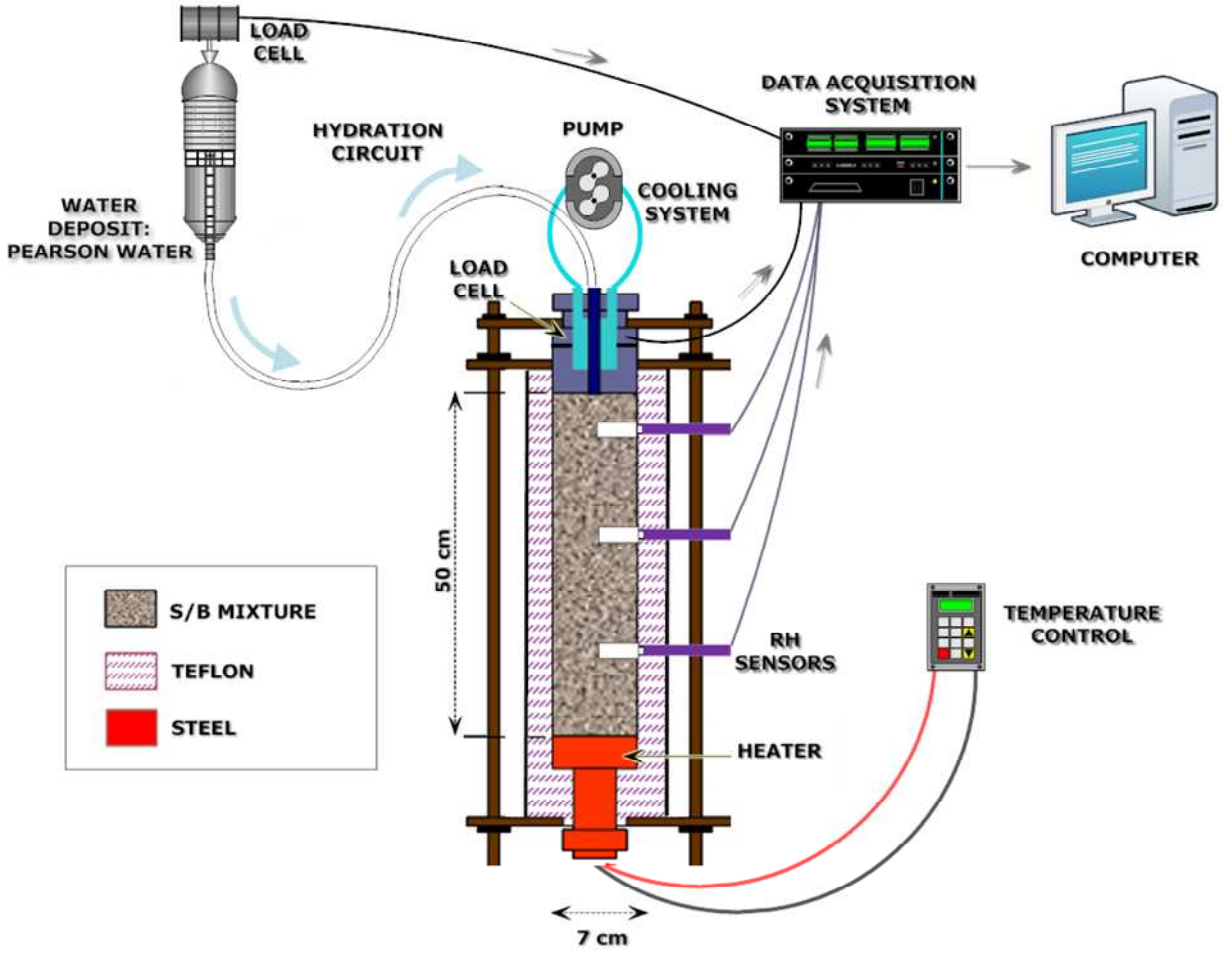

Figure 5: Experimental setup for the infiltration test (for the exact location of sensors see Figure 4)

4 Methodology

4.1 FABRICATION OF THE COLUMN

The column was manufactured by filling the cell in seven 7-cm high layers. The material was just poured inside the cell. The quantity of material was computed taking into account the initial water content, the inner volume of the cell (7 cm in diameter and a target height of 50 cm) and the target dry density, which was 1.45 g/cm^3. Very low compaction energy was applied to the mixture: 5 to 10 strokes with a 2.5-kg Proctor rammer with a 30.5 cm drop to each of the 7 layers (Figure 6, left).

Between the mixture and the upper closing, a 70-mm diameter and 8-mm high porous stone was placed. The top plug with the o-rings around was pushed to its place and tightened. This assembly was weighed and afterwards, the perforations for the insertion of the sensors were drilled in the mixture through the Teflon walls. The assembly was weighed again in order to know how much material had been lost as a consequence of drilling. Thus the initial characteristics of the column were obtained (Table 2). The differences with respect to the target values are due to the compression of the column caused by the upper plug tightening. Figure 6 (right) shows the aspect of the cell in its final configuration.

Table 2: Characteristics of the sample after compaction

	S/B
Initial water content (%)	3.6
Sample mass (g)	2949
Sample mass after drilling (g)	2930
Volume of sensors (cm^3)	18
Theoretical dry mass (g)	2828
Diameter (mm)	70.4
Height (mm)	497.6
Dry density (g/cm^3)	1.47
Porosity	0.456
Void ratio	0.839
Degree of saturation (%)	12

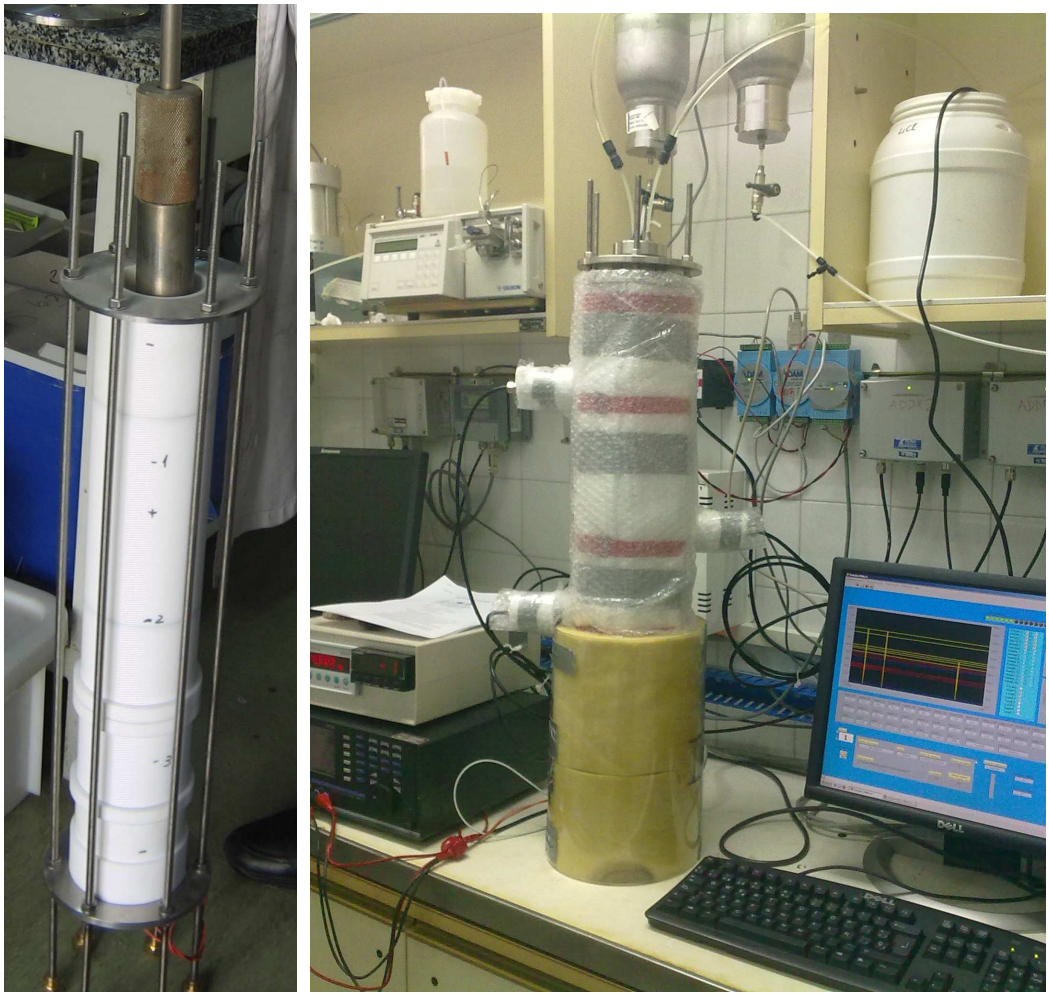

Figure 6: Cell during compaction of the mixture (left) and in operation with the external isolation material (right)

4.2 TESTS INITIATION

Once the cell was mounted and the sensors inserted, the data acquisition was launched. A brief period to check the initial stabilisation and the correct working of the sensors was taken. This period lasted 260 h. The temperatures recorded by the three sensors were nearly identical and reflected the laboratory changes. For the relative humidity the differences among sensors were below 1%, with an average value of 46% (Figure 7).

The valve giving access to hydration was accidentally opened for a few minutes (about 5 min), and due to the high permeability of the material, this caused the relative humidity in the upper part of the column to increase. The average water content of the column increased from 3.6 to 4.7%.

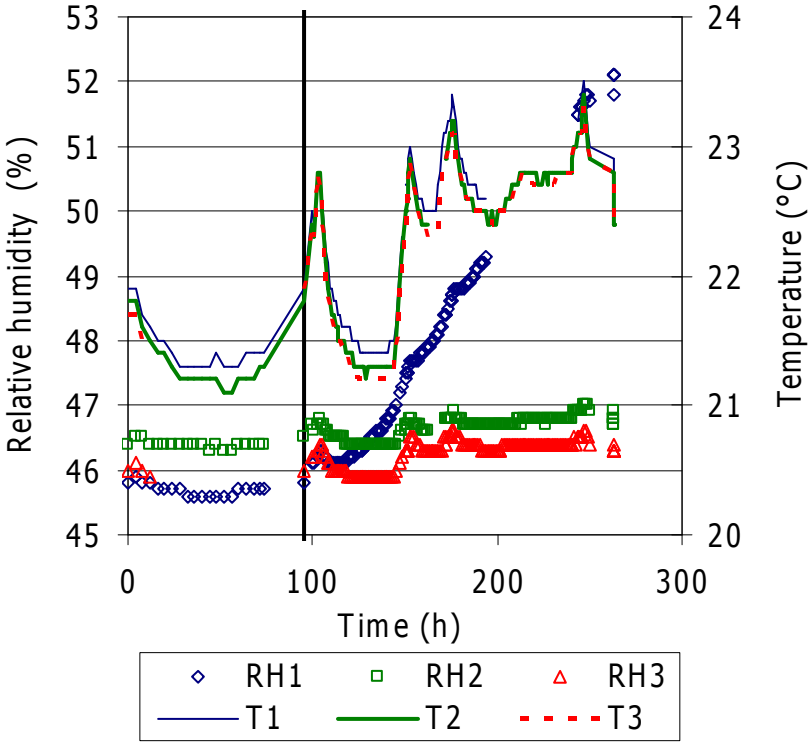

Figure 7: Sensors readings before initiation of the test (sensor 1 placed at 40 cm from the bottom, sensor 2 at 22 cm and sensor 3 at 10 cm). The thick vertical line indicates the accidental opening of the hydration line

5 Online results

5.1 INITIAL HEATING

The heater and the cooling system on top were switched on 260 h after starting data acquisition, and this time is considered as t=0 for the rest of the test. The target temperature of 100°C was reached in 25 min, but the stabilisation of the temperature registered by the sensors took approximately 30 h, and much longer for the relative humidity (Figure 8). After 7 h of heating the cell was wrapped with an isolating material and this was clearly reflected in an increase of the temperature inside the mixture and affected as well the relative humidity. After 1566 h the isolation material was changed, and again modified after 1666 h, which improved

the longitudinal heat transmission inside the column and caused a temperature increase of almost 10°C at 10 cm from the heater (sensor 3) (Figure 9, left). The relative humidity inside the cell reflected also the improvement of the isolation system and the ensuing increase of temperature in the mixture (Figure 9, right). As well, the laboratory temperature changes were subsequently less reflected in the temperatures inside the material. The two sensors farther from the heater reflected an increase in relative humidity from the beginning of heating, more intense for the middle sensor from the moment the temperatures near the heater increased. Both sensors recorded a stable and similar RH value approximately after 2200 h. However, the sensor placed at 10 cm from the heater recorded a sharp initial increase up to a value of RH 70%, and after 120 h this value started to decrease, more intensely when the isolation was improved. A quasi-stable value of 36% was reached after 2400 h. This evolution of the relative humidity along the column reflected the migration of water vapour from the material close to the heater towards cooler zones.

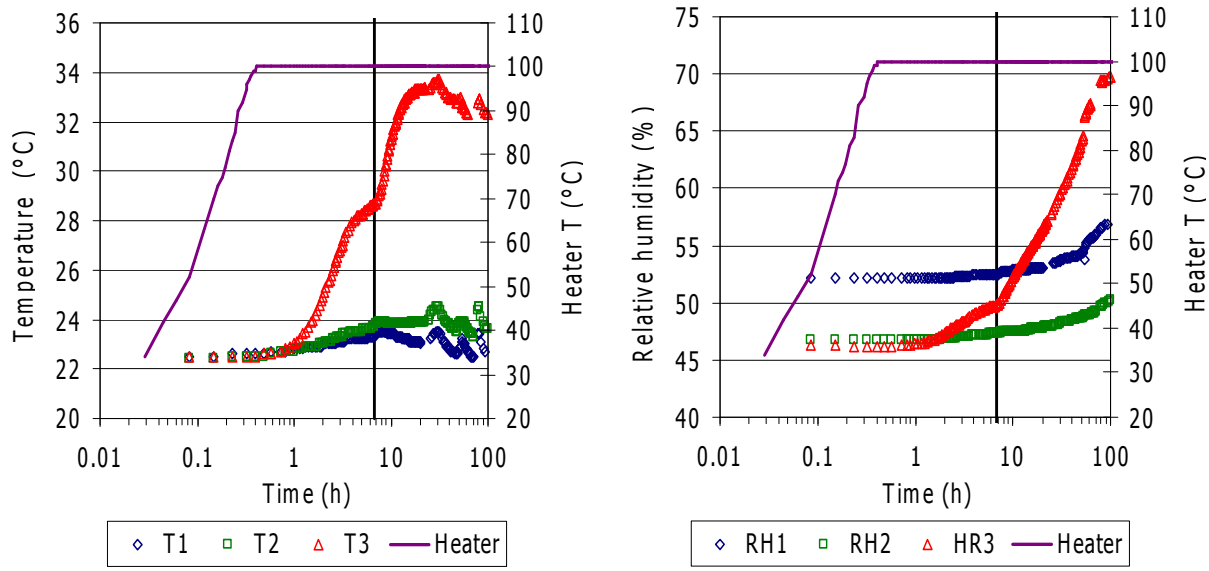

Figure 8: Evolution of *T* and RH after setting the heater to 100°C (sensor 1 placed at 40 cm from the bottom, sensor 2 at 22 cm and sensor 3 at 10 cm). The thick vertical line indicates the wrapping of the cell with the first isolating material

Once the relative humidity inside the column stabilised, the heater temperature was increased to 140°C, which was the final target temperature. This process took 12 min. The temperatures inside the mixture stabilised after 24 h, and the relative humidity in approximately 1130 h (Figure 10).

The equilibrium values of *T* and RH at the end of the heating phases with heater temperature 100°C and 140°C are shown in Figure 11.

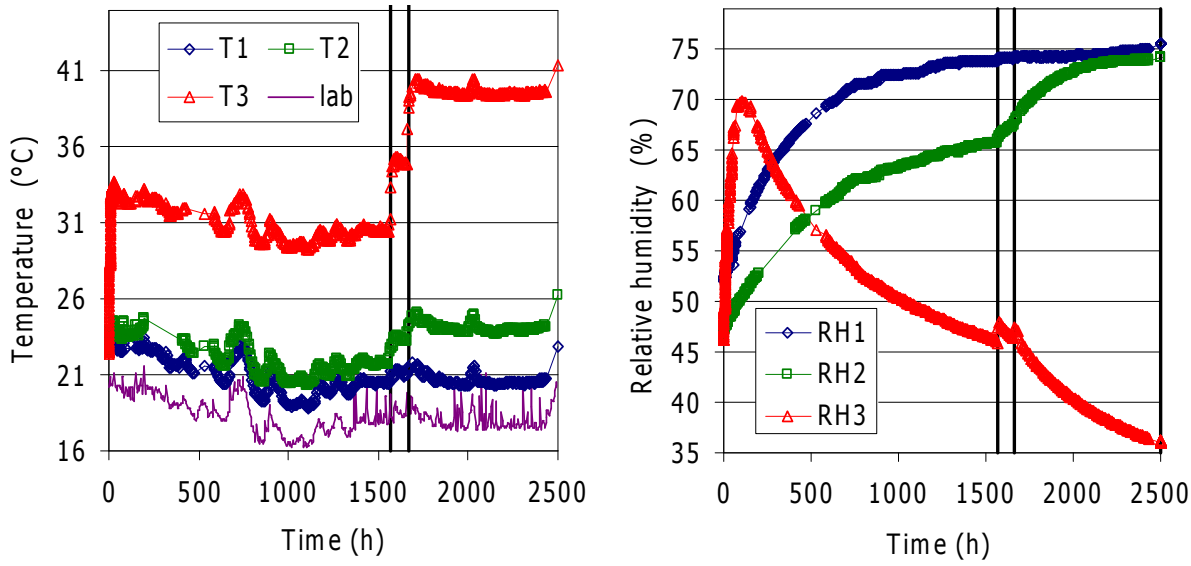

Figure 9: Evolution of *T* and RH during the phase in which the heater was set to 100°C (sensor 1 placed at 40 cm from the bottom, sensor 2 at 22 cm and sensor 3 at 10 cm). The thick vertical lines indicate improvements in the isolation system

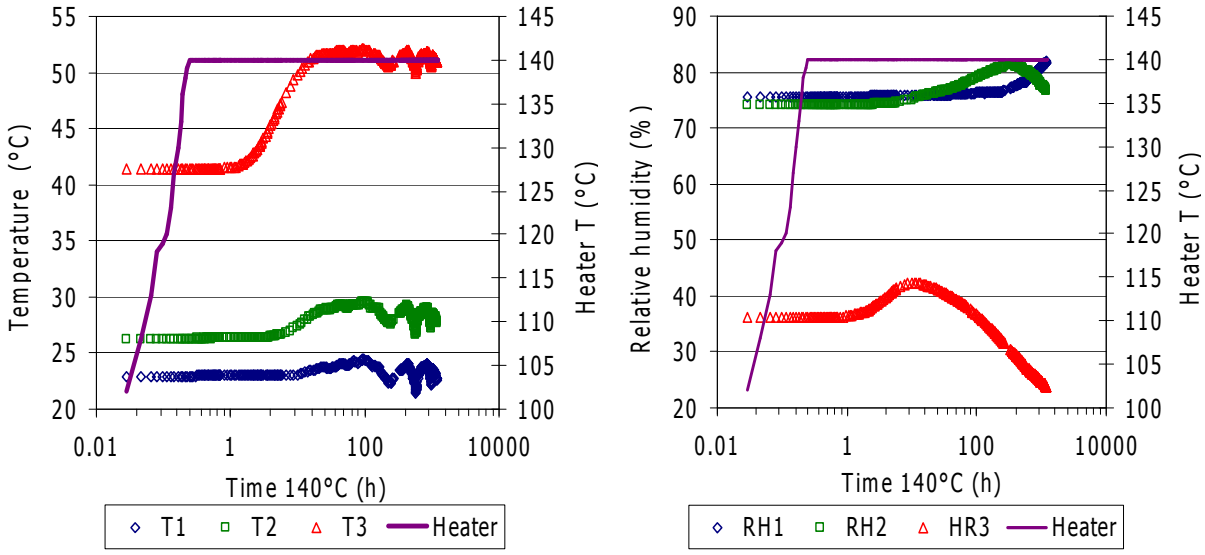

Figure 10: Detailed evolution of *T* and RH in cell S/B as the heater *T* increased from 100 to 140°C (sensor 1 placed at 40 cm from the bottom, sensor 2 at 22 cm and sensor 3 at 10 cm)

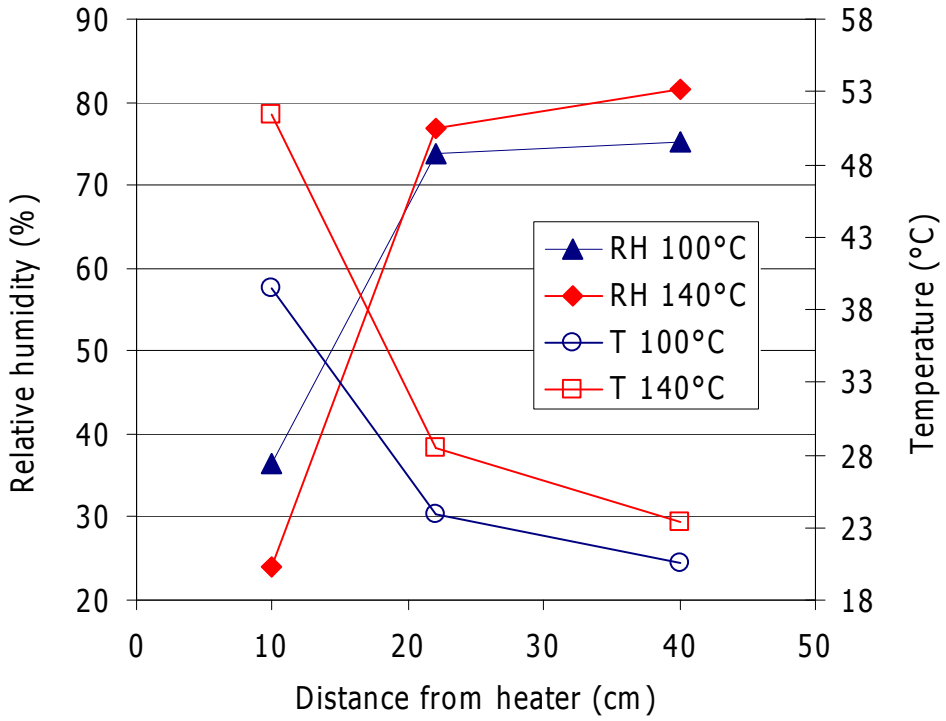

Figure 11: Equilibrium values measured inside the material when the heater temperature was 100°C (*t*=2400 h) and 140°C (*t*=3620 h)

5.2 HEATING AND HYDRATION

After the stabilisation of RH and *T* for a heater temperature of 140°C, the hydration line was opened. Only a small pressure, equivalent to a 60-cm high water column, was applied to the saturation water.

Figure 12 shows the evolution of *T* and RH recorded by the sensors at the beginning of hydration. The temperatures kept the same as before hydration for some days. As the water front approached the sensors, the temperatures started to increase, so the simultaneous increase in temperature and relative humidity took place first in sensor 1 (after approx. 44 h), then in sensor 2 (after approx. 160 h) and finally in sensor 3 (after approx. 235 h). The coupling between the increase in water content and that of temperature can be clearly seen in the Figure. For sensor 3, placed in the hottest area, the arrival of the water front caused a temporary decrease in temperature that was quickly recovered. The overall increase in temperature due to the increase in water content was of 6°C for sensor 1, 14°C for sensor 2 and 16°C for sensor 3.

Figure 13 shows the evolution of temperature and relative humidity inside the column and the water intake until the end of the test, which was dismantled after 1023 days (24551 h) of hydration. The temperatures inside the material kept steady, oscillating according to the laboratory temperatures, particularly in the upper part of the column. Thus, for sensor 1 the average steady temperature was 27±2°C, for sensor 2 was 40±2°C and for sensor 3 was 63±1°C. The latter stopped working after approximately 19000 h of hydration, while sensor 2 started at this time to record some erratic values (not taken into account to compute the average temperature). With respect to the RH evolution, its increase was very sudden once the water front reached the area where the sensors were placed. Consequently the sensors became quickly flooded and later started to record faulty values or signs of internal water condensation

(except for sensor 1 which recorded a RH value of 98%). Sensor 1 started recording 98% approximately 135 h after hydration started, sensor 2 after 235 h and sensor 3 after 387 h. The overall water intake was also very large until the bottom sensor became flooded, and then the water intake rate softened (continuous line in Figure 13, right). In fact, air bubbles could be seen in the hydration line, and these were periodically purged, since they seemed to hinder the water inflow. This is the reason why the water intake curve is not smooth, because after purging, the water intake was temporarily accelerated. In order to simplify the air purging process, a syringe was connected to the hydration circuit (Figure 14, left). It is considered that this could have given place to some unnoticed leak that caused the water intake measurement to be overestimated (see below).

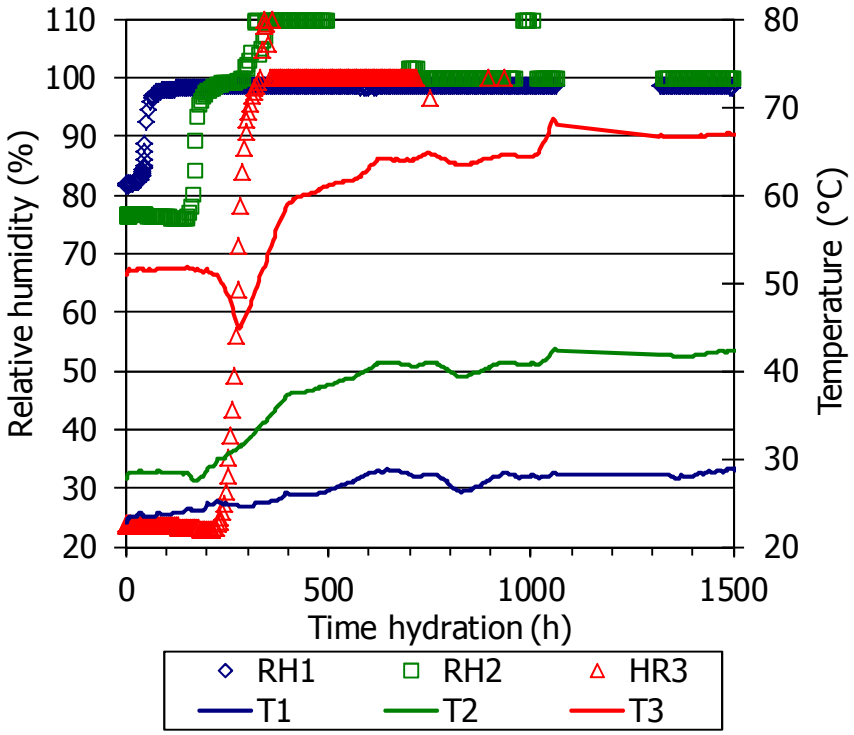

Figure 12: Evolution of *T* and RH in cell S/B after the beginning of hydration (sensor 1 placed at 40 cm from the bottom, sensor 2 at 22 cm and sensor 3 at 10 cm). Values above 100% are faulty

The temperatures on the surface of the cell were measured periodically after one year of operation with thermocouples placed on the surface of the cell, i.e. on the Teflon, at the same levels as the sensors inserted in the column but on the opposite side of the column (Figure 14, right). As well, the temperatures on the surface of the isolating material were measured at the same height (Figure 15). There is a slight trend for these temperatures to decrease over time, which could be related to the increase in thermal conductivity with the increase in water content, but also to changes in the lab temperature. Figure 16 shows the average of these temperatures from June 2013 (when the first external measurements were taken) to February 2015 (end of test) at the different positions measured. It can be observed that the decrease of temperature from the inside of the mixture to the external surface of the Teflon cell is not significant, which highlights the good lateral isolation of the cell and guarantees the uniaxial geometry of the thermal gradient (the isotherms would be parallel to the heater surface). The same values are plotted in Figure 17 as a function of the distance from the heater, which allows to visualise the steep thermal gradient along the column.

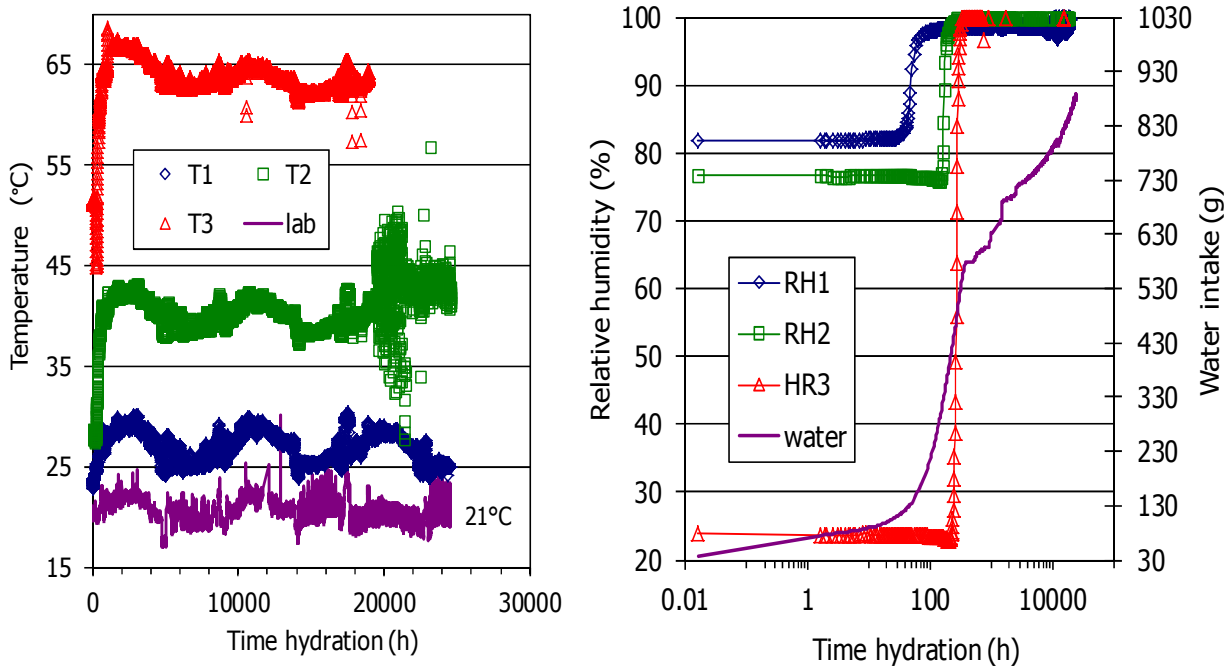

Figure 13: Evolution of *T* (left) and RH (right) in cell S/B during the hydration phase (sensor 1 placed at 40 cm from the bottom, sensor 2 at 22 cm and sensor 3 at 10 cm)

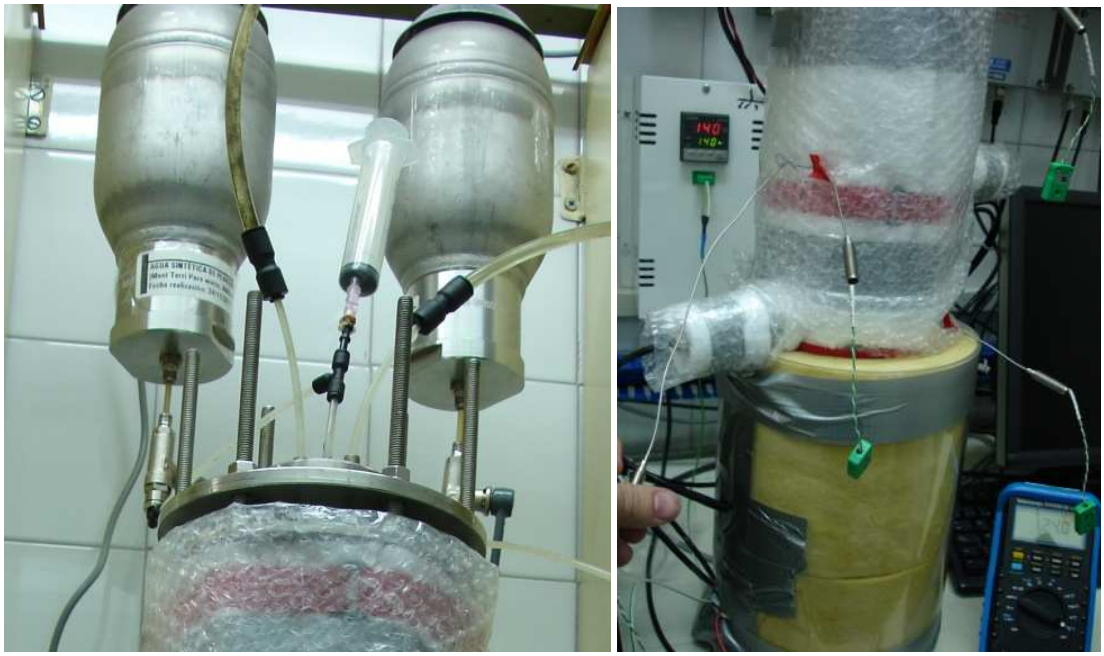

Figure 14: Hydration system with syringe connected for extracting air bubbles (left) and thermocouples installed on the cell surface and on the surface of the isolating material (right)

The heater power was also measured during all the test phases. The improvement of the isolation induced a decrease of the heater power from 10.7 to 6.6 W to keep the target temperature of 100°C at the heater surface. When the heater temperature was increased to 140°C, the heater power increased to 10 W. Upon hydration, the arrival of water to the heater area gave place to a progressive increase in heater power up to a value of 12 W, which remained approximately constant (12.2±0.4 W) until the end of the test (Figure 18).

A summary of the values recorded during the whole hydration phase is given in Appendix 1.

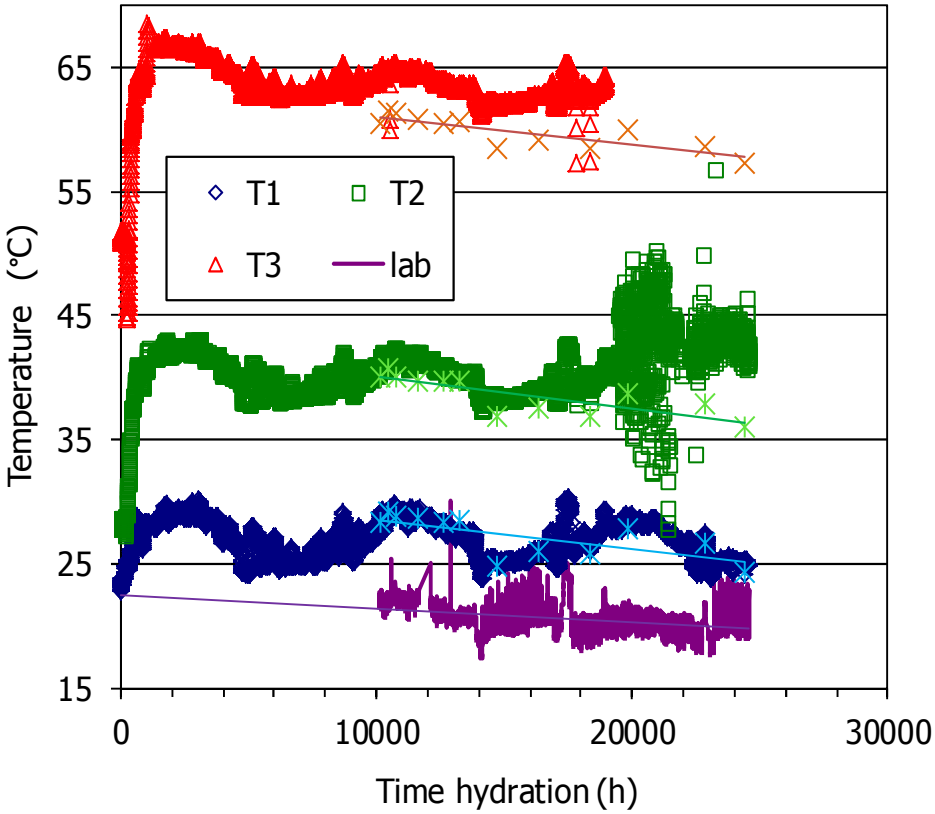

Figure 15: Evolution of temperature inside the column and on the Teflon surface (crosses) during the hydration phase (T1 at 40 cm from the bottom, T2 at 22 cm and T3 at 10 cm)

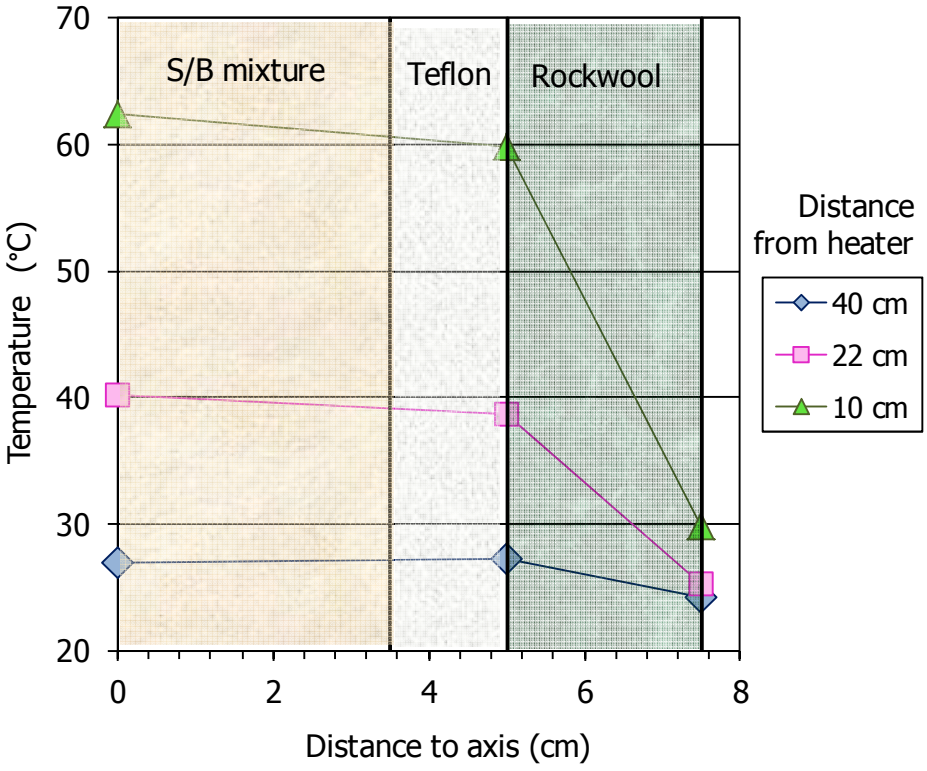

Figure 16: Average temperatures at different distances from the heater measured by the sensors inside the cell and by external thermocouples from June 2013 to February 2015 (average laboratory temperature in this period 20.6±1.3°C)

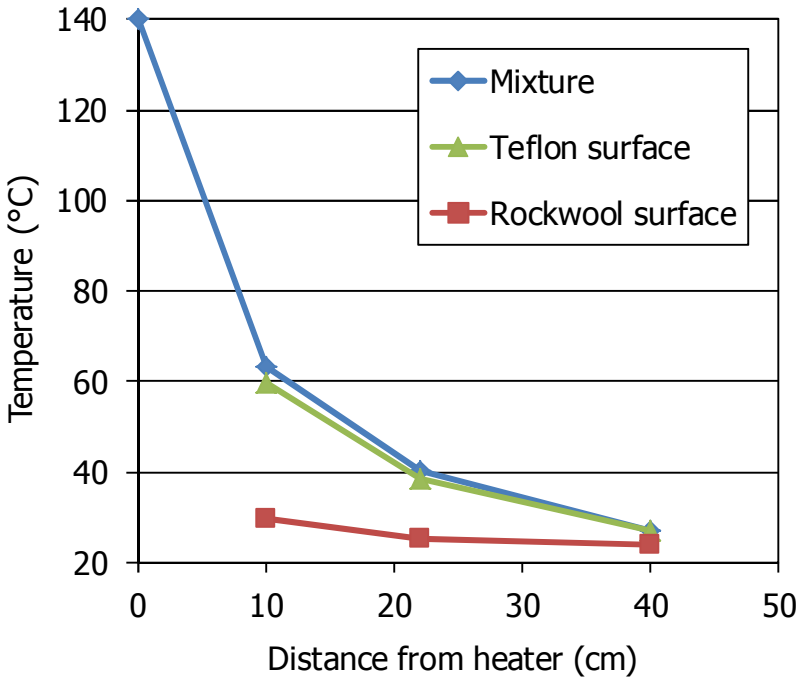

Figure 17: Average temperatures along the column S/B measured by the sensors inside the cell and external temperatures measured with thermocouples from June 2013 to February 2015

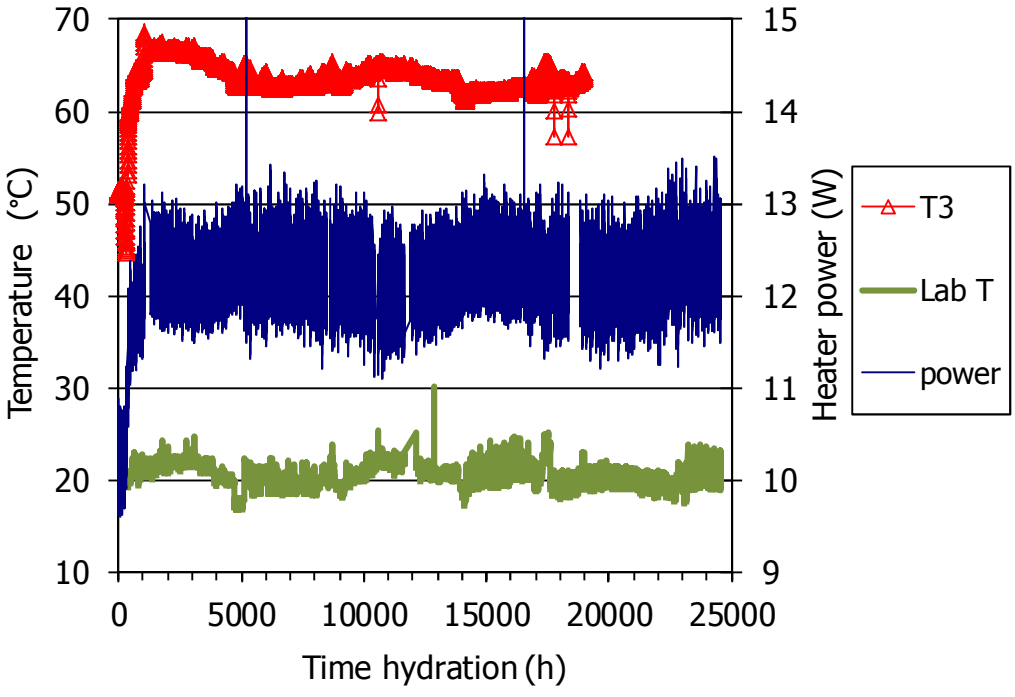

Figure 18: Laboratory temperature, heater power and temperature at 10 cm from the heater (sensor 3) in cell S/B during the hydration phase of the test

6 Dismantling

6.1 SWITCHING OFF

After 1023 days of hydration (1177 days since the beginning of the test), the cell was dismantled. For that, the water inlet was closed and the heater was switched off, the isolation material was removed (Figure 19) and the sensors extracted. Upon extraction, water dripped from the hole of sensor 1 (Figure 20). The appearance of the sensors was good and they did not look damaged (Figure 21), although sensor 3 was not providing any information and sensors 1 and 2 were not measuring RH. Figure 22 shows the evolution of temperature inside the mixture once the heater was switched off and until the sensors were extracted. It can be observed that the temperature decreased quickly to values close to the laboratory temperature.

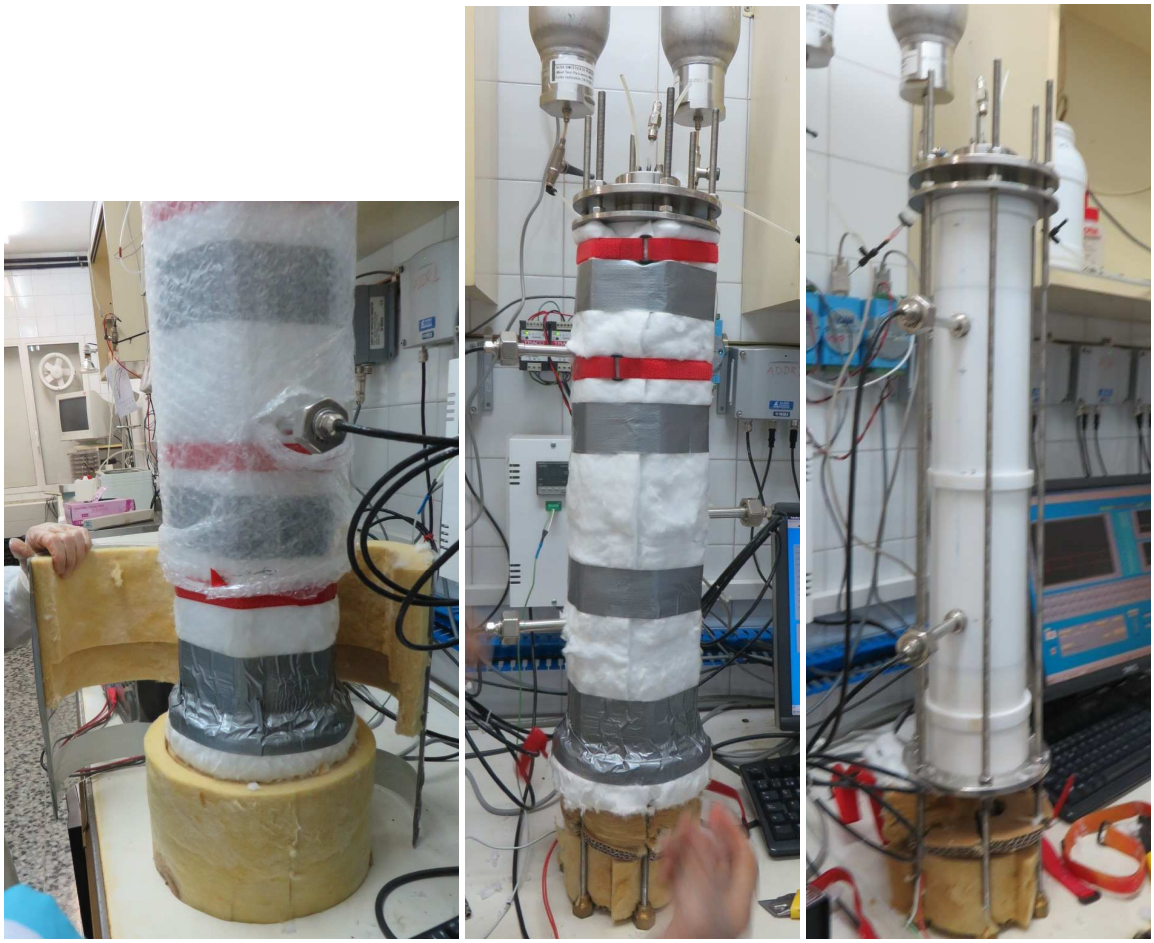

Figure 19: Removal of the isolation material

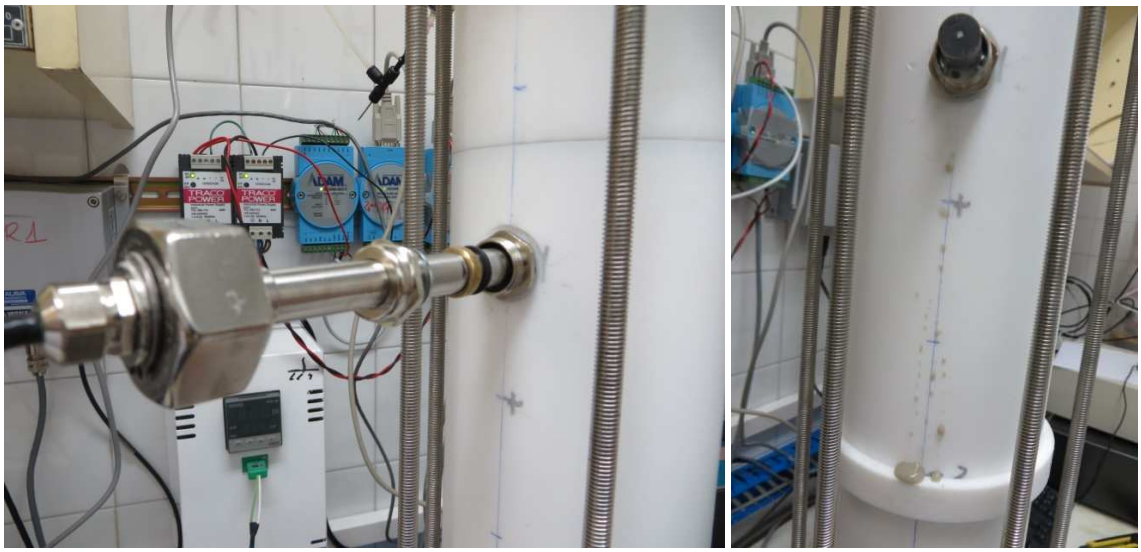

Figure 20: Extraction of sensors (left) and water drip through the sensor hole (right)

Figure 21: Appearance of sensor 1 (top) and sensor 3 (bottom) after extraction

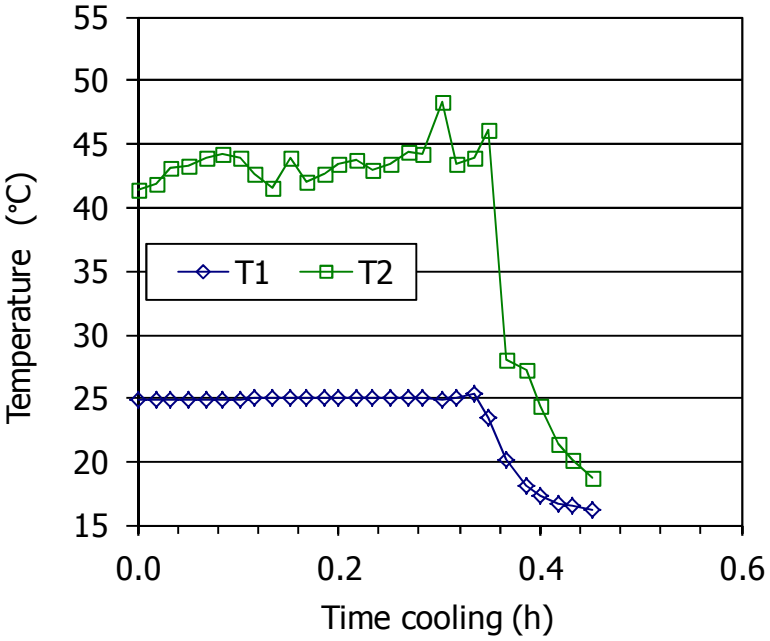

Figure 22: Evolution of temperature inside the mixture from the moment the heater was switched off to the extraction of the sensors (T1 at 40 cm from the bottom, T2 at 22 cm)

The final state of the sensors was checked by letting them measuring after extraction. It must be recalled that the three of them seemed to be flooded and did not give any relative humidity value. Sensors 1 and 2 recovered and indicated relative humidity and temperature values close to ambient, but different between the two sensors. Sensor 3 did not record any value. The three sensors were dismounted and cleaned, and afterwards, the values recorded by sensors 1 and 2 were similar between them, which would indicate that their filters were differently contaminated. Sensor 3 recorded also a similar temperature, but it was not able to give any relative humidity value (Figure 23). Apparently it had been irreversibly damaged during operation.

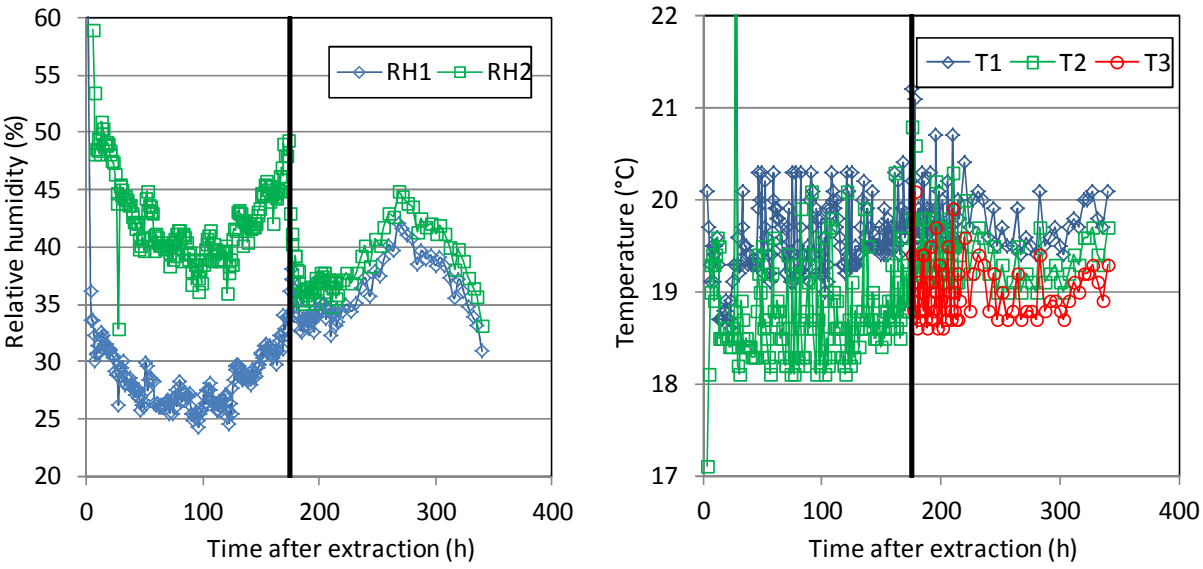

Figure 23: Sensors' recordings after their extraction from the cell (the thick vertical line indicates the moment they were cleaned)

6.2 EXTRACTION OF THE COLUMN AND SAMPLING

The mixture was extracted out of the column in four pieces, taking advantage of the different Teflon elements. Each piece had a cohesive consistence and the cylindrical form of the cell, from the top (Figure 24) to the bottom (Figure 25), with a uniform appearance all along the column. Only the two centimetres closest to the heater were loose and very dry, although some fragments were consistent (Figure 26). The rest of the column could be easily handled and subsampled in 2-cm thick sections, as shown in Figure 27.

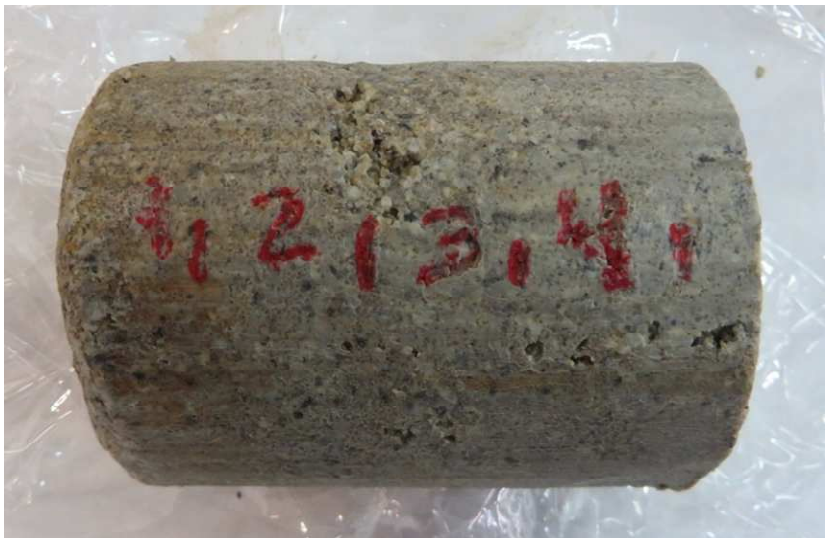

Figure 24: Appearance of the upper part of the column (9 cm) after extraction

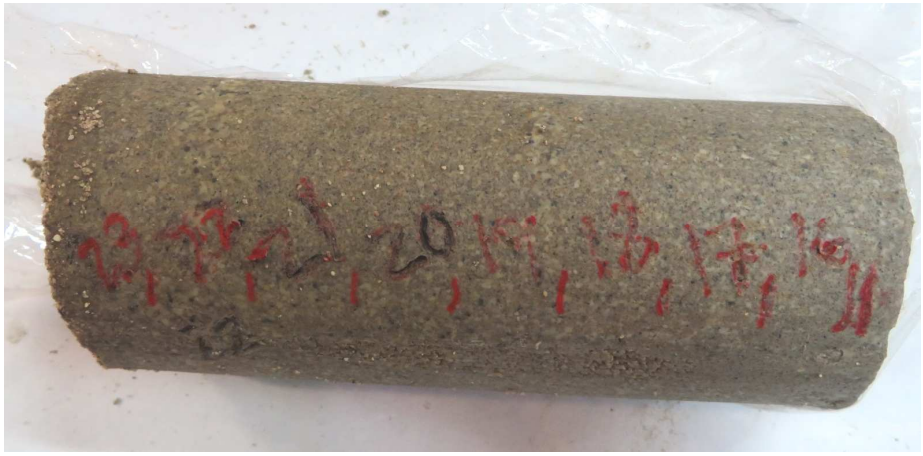

Figure 25: Appearance of the bottom part of the column (except the 2 cm closest to the heater) after extraction

The final height of the column was 49.76 cm and its diameter was on average 7.05 cm, although it tended to increase from the bottom part of the column to the top. The diameter was measured at different positions along the column once extracted (Figure 28). The internal diameter of the Teflon elements constituting the cell was measured as well at different positions. The values are shown also in Figure 28 and indicate that the Teflon was slightly deformed by the swelling of the mixture towards the upper part of the cell.

Figure 26: Appearance of the column section closest to the heater (section 24)

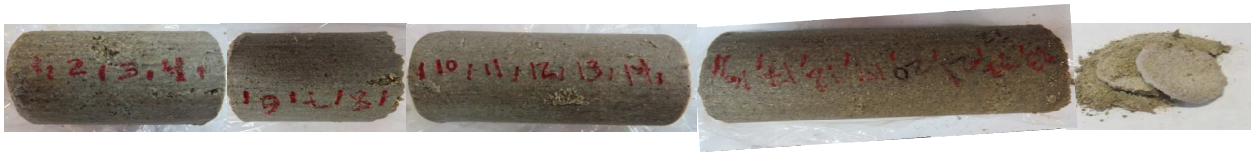

Figure 27: Subsampling in sections along the column, from top (section 1) to bottom (section 24)

The final weight of the column was 3625.06 g. Hence, taking into account the initial values indicated in Table 2, the final average water content and dry density of the column were 28.2% and 1.46 g/cm^3. This meant also that the total water intake was 676 g, much below the value recorded by the load cell weighing the water deposit, which was 887 g (Figure 13). This observation confirmed that the hydration system leaked once the purging system was installed.

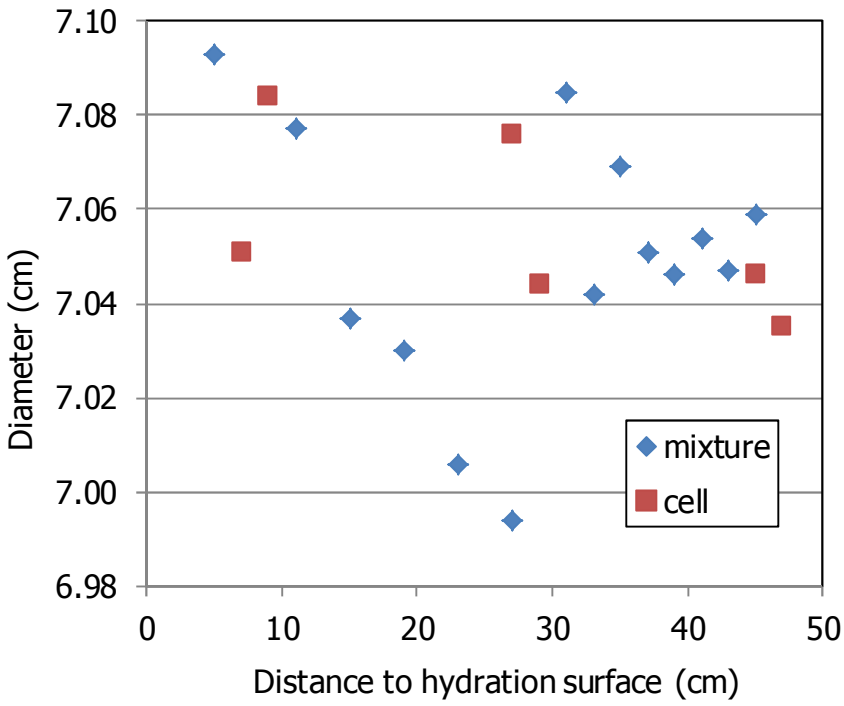

Figure 28: Final diameter of the column (mixture) and internal diameter of the Teflon elements (cell)

6.3 POSTMORTEM ANALYSES

Once extracted the column was subsampled in 24 sections approximately 2 cm in thickness. The material of each section was used in the following way:

- a cohesive fragment of each section was used to determine its volume by immersing it in mercury,
- another portion was used to determine the water content by oven drying to 110°C for 48 h,
- a small fragment was lyophylised and its pore size distribution determined by mercury intrusion porosimetry,
- the remaining sample of each section was kept for possible subsequent analyses.

The results of these determinations are presented below.

6.3.1 Water content and dry density

The water content of the subsamples was determined using between 50 and 125 g (average 70 g) of wet sample, which were dried in the oven to 110°C for 48 h to determine the mass of dry sample. Adjacent cohesive fragments of the mixture were trimmed to a regular shape, weighed and immersed in mercury to determine their volume and hence, bulk density. The volume of these samples was between 13 and 44 cm^3 (average 29 cm^3). It was observed that some mercury could remain in the pores of the samples after immersion and, due to health security issues, these samples were not dried in the oven. The water content determined in the adjacent samples of the same section was used to compute the dry density. The values thus obtained along the column are shown in Figure 29. From these, the degree of saturation of each sample was computed and the values shown in Figure 30 were obtained. It can be observed that the values for the three parameters, dry density, water content and degree of saturation, are similar along the column, and they only change significantly in the proximity to the heater, where the water content is much lower and the dry density higher. The results for each sample are presented in Table A- IV of Appendix 2. The average water content computed from these measurements was 28.3% and the dry density 1.44 g/cm^3, corresponding to an average degree of saturation of 89%. This average water content was similar to that determined from the difference between the final and the initial weight of the column (28.2%, see "Extraction of the column and sampling"), but the dry density was lower (1.44 *vs*. 1.46 g/cm^3). This reduction in the dry density of the subsamples is usually observed when it is determined in trimmed subsamples and can be attributed to the changes in density caused by subsampling and trimming. This fact, along with the slight drying that the samples might have experienced during manipulation could give place to degrees of saturation lower than the ones the mixture actually had before extraction of the column.

If the section in contact with the heater is excluded from the computation of average values, they would be 30.5±1.9% for water content, 1.43±0.04 g/cm^3 for dry density and 93±4% for degree of saturation, all of them quite homogeneous, exhibiting no trend along the column.

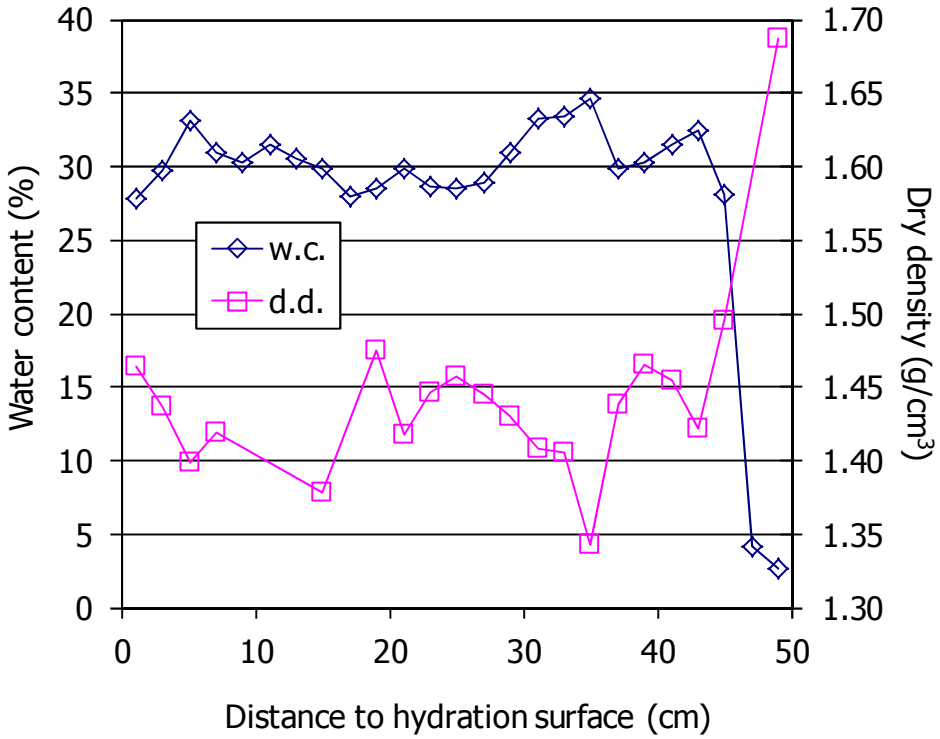

Figure 29: Final water content and dry density along the column as determined in subsamples

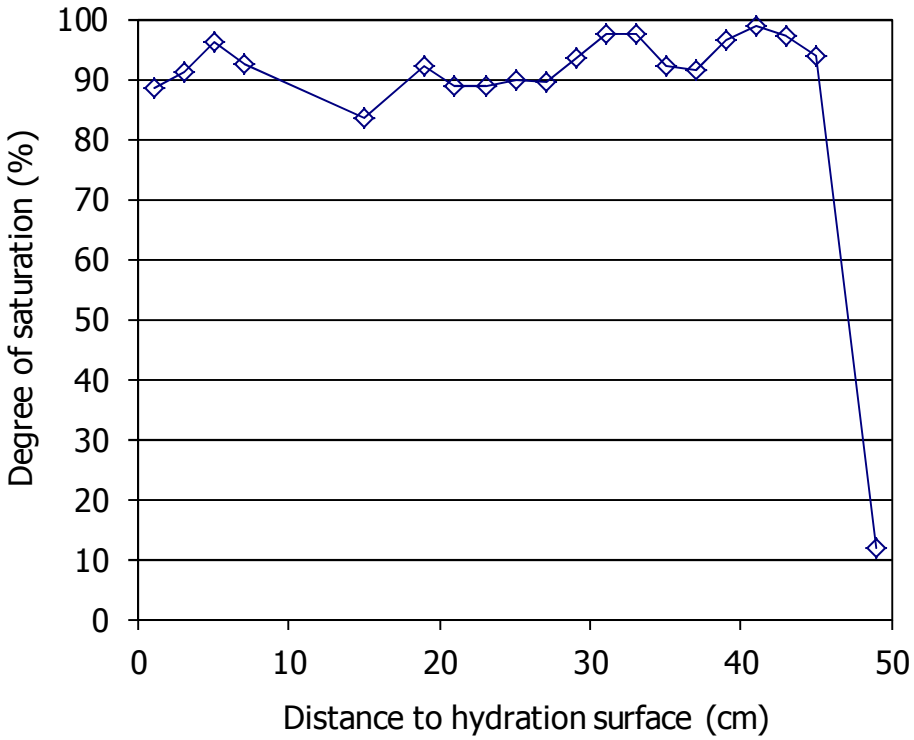

Figure 30: Final degree of saturation along the column as determined in subsamples

6.3.2 Pore size distribution

Fragments of each section of volumes comprised between 0.6 and 1.1 cm^3 were analysed by mercury intrusion porosimetry (MIP). The samples were put in the ice condenser of a Telstar LioQuest equipment at -50°C for 3 h. Afterwards they were lyophilised for 19 h at a

temperature of -50°C under a vacuum of 0.2 mbar, so that to eliminate the water in the pores by sublimation. Afterwards, the samples were kept in desiccators until the MIP tests. The porosimeter used was a Micromeritics AutoPore Series IV 9500, which applied a maximum injection pressure of 31900 psi, allowing the exploration of pore diameters between 0.007 and 500 µm. Prior to mercury injection the sample was outgassed by applying a vacuum of 50 µm-Hg. Afterwards the mercury injection pressure was increased from 0.36 to 31900 psi in 110 steps. To determine the extrusion branch of the curve, the pressure was released in 57 steps down to a pressure of 4.44 psi. A contact angle of mercury of 139° both on advancing and of receding on the clay surface was considered.

The mercury does not intrude the microporosity (pores of a size of less than 0.002 µm, according to the classification of Sing *et al*. 1985), but only the macroporosity and part of the mesopores. The percentage of pores not intruded by mercury includes not only those whose sizes are above 500 µm or below 0.007 µm, but also those whose entrance pore size is below the latter value or those isolated, even if the pores themselves are larger. The percentage of pores not intruded can be computed by comparing the actual void ratio of the samples (computed from their dry density and solid specific gravity measured by pycnometers) and the apparent void ratio calculated from mercury intrusion. The pore size distribution curves obtained taking this correction into account are shown in terms of incremental pore volume in Figure 31. For the sake of clarity only a few of the samples analysed are represented, because the results were similar for all the samples except for the two closest to the heater.

Assuming that the percentage of pores not intruded corresponds entirely to the <7 nm size, an estimation of the percentage of micropores was computed and the percentage of each pore size recalculated (Figure 32, left). The percentage of the porosity intruded by the mercury was fairly high (88±7%), this meaning that the volume of pores with a size of less than 7 nm or not interconnected, which have been considered micropores, was not very large. The mode of the macropores and mesoporos for each sample is shown in Figure 32 (right). The results detailed for each sample are included in Table A- V of Appendix 2. A summary of these results is presented in Table 3, where the results for the original material are also included (Villar 2013). No trends along the column were observed with respect to the pore size distribution, and thus, just the average values for sections 1 to 23 are given in the Table. The results for the two samples taken in section 24 (2 cm closest to the heater) are given separately. They had less macropores, but they had a larger size, and more micropores. After saturation the percentage of macropores as well as their size decreased with respect to the original material, whereas the percentage of micropores increased. This could be explained by the swelling of the bentonite.

Table 3: Summary of the pore size distribution results obtained by MIP

Sample	Macropores (>50 nm), %	Mode macropores, µm	Mesopores (50-7 nm), %	Mode mesopores, nm	Micropores (<7 nm), %
Original	92	204	8	19	
Sections 1-23[a]	83±6	58±21	5±1	16±4	12±7
Section 24[b]	53	110	8	18	39

[a]23 samples; [b]2 samples

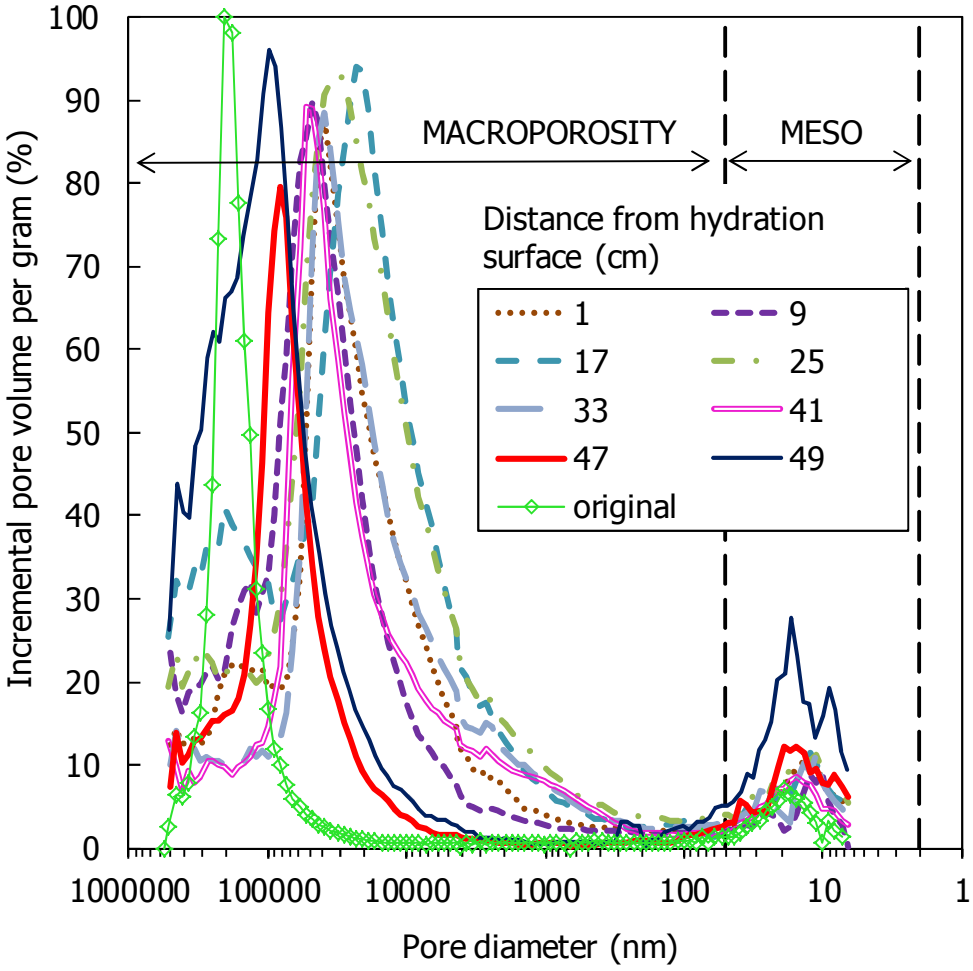

Figure 31: Incremental pore volume for some of the samples analysed and for the original material

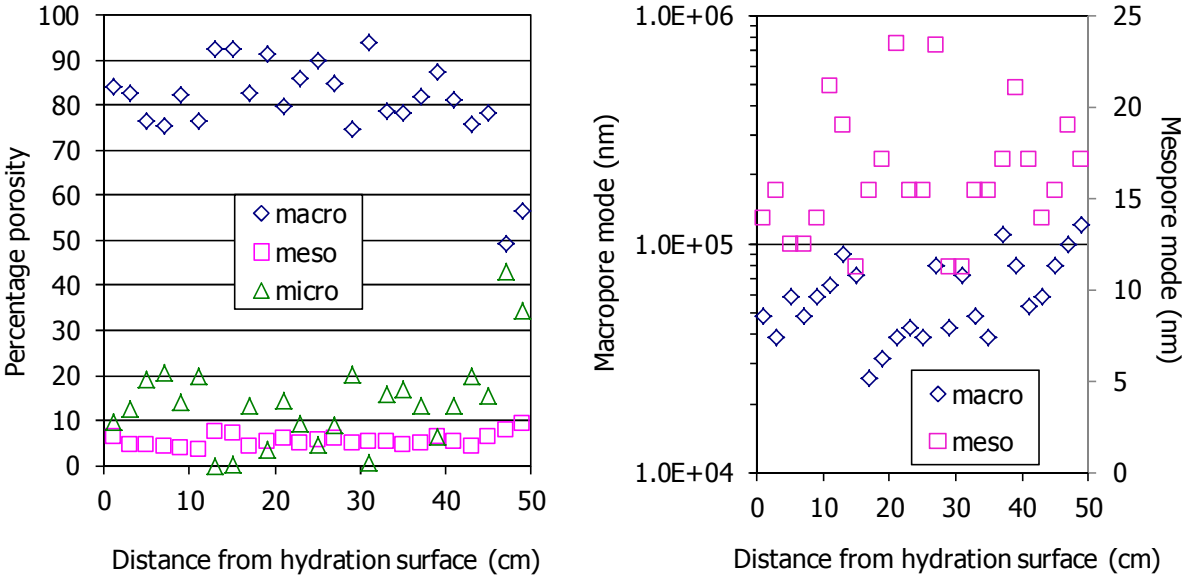

Figure 32: Final pore size distribution along the column in terms of size percentage (left) and pore mode (right)

6.3.3 Scanning electron microscopy observations

Specimens taken from three sections of the column (1, 10 and 24) were observed in a scanning electron microscope (SEM) ZEISS EVO LS 15, with an energy dispersive X-ray spectrometer (EDS) coupled. Before observation the samples were covered under vacuum with a gold coating to make them electrically conductive. The overall aspect of the three of them was dominated by the quartz grains of the sand and scattered patches of smectite, which according to the semi-quantitative analyses performed with the EDS system, had a high Fe content.

Sections 1 and 24 (farthest and closest to the heater, respectively) had abundant chloride and sulphate crystals or impregnations. Surprisingly, these were not observed in section 10, located towards the middle of the column. These observations must be considered carefully, since they correspond to very small fragments of samples that might not represent their average characteristics.

Figure 33 shows the assemblage of quartz grains covered by chloride with a glossy appearance and cube-shaped NaCl crystals in section 1. Sulphate crystals were frequently found precipitated on the smectite, normally calcium sulphates but also Ca-Na ones (glauberite?), as well as Fe-rich carbonates (Figure 34).

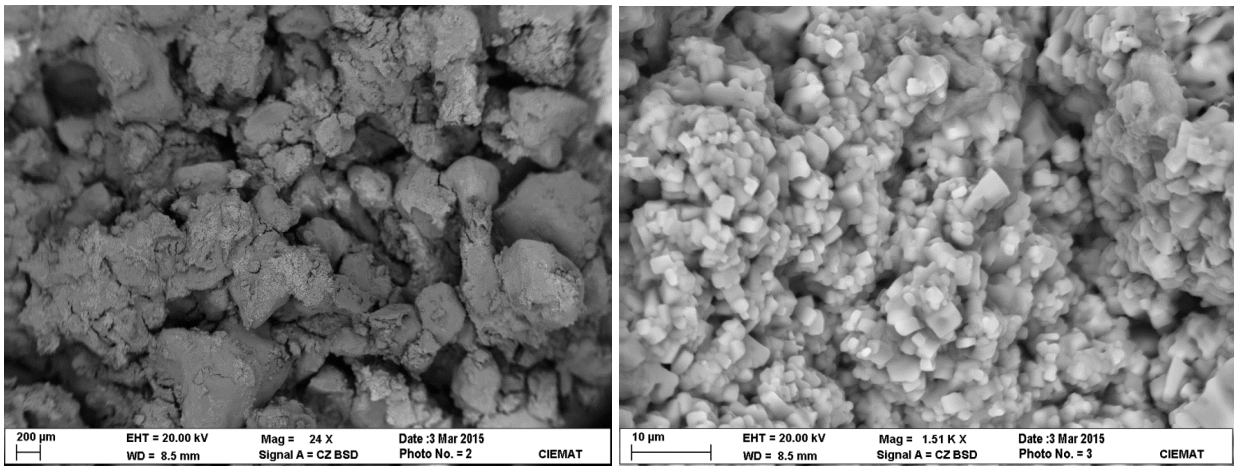

Figure 33: Section 1. General appearance of quartz grains with a glossy superficial covering of chlorides (left) and NaCl crystals (right)

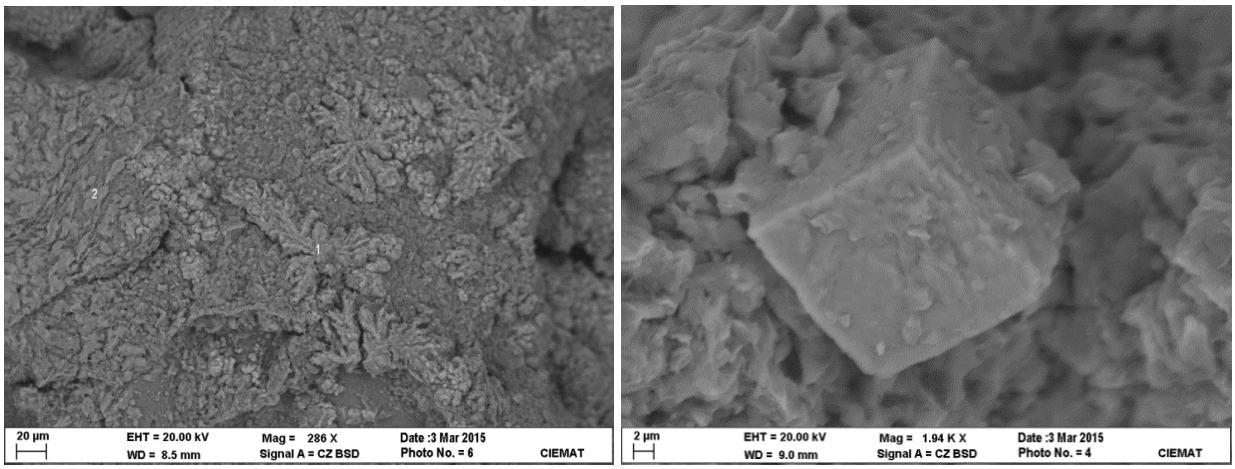

Figure 34: Section 1. Smectite covered by Ca (and Na) sulphates (left) and crystal of Fe (and Ca and Mg) carbonate (right)

The sample of section 24 (closest to the heater) showed layers of sodium chloride overlapping quartz grains or smectite particles, as well as NaCl crystals of different sizes and shapes (Figure 35). Sulphates were often found, sometimes covered by NaCl sheets or fibers of Ca-sulphate. Rhomboidal crystals or plates of Ca-Na sulphates (glauberite?) were also observed (Figure 36).

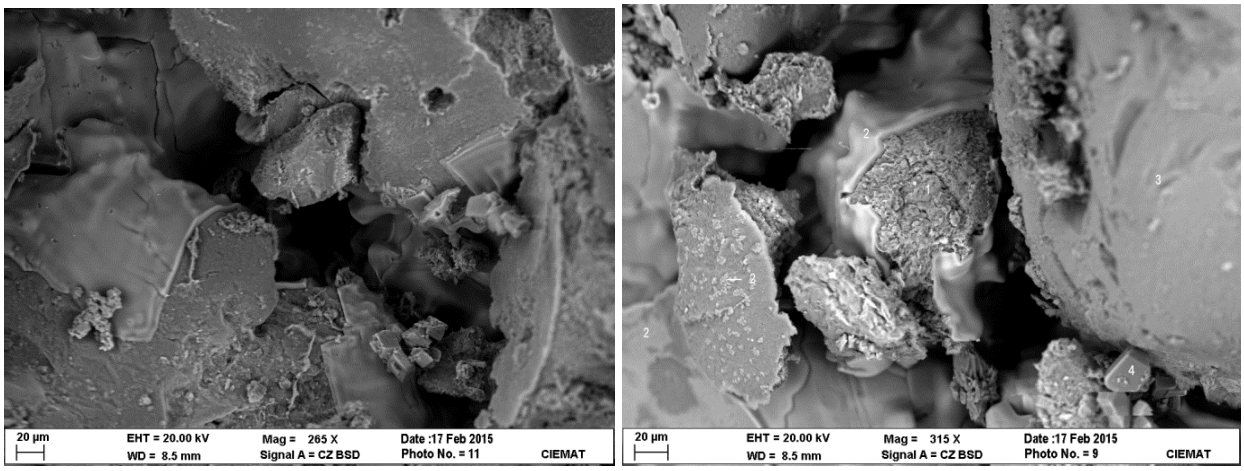

Figure 35: Section 24. NaCl as thin layers and crystals (left) and various minerals (1: smectite, 2: NaCl as thin layer or small crystals, 3: quartz, 4: glauberite) (right)

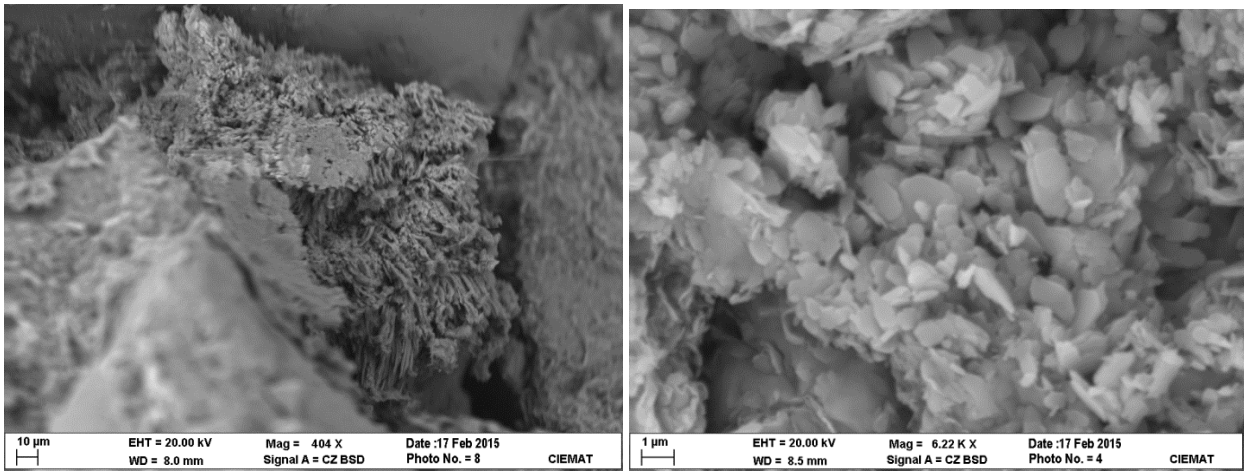

Figure 36: Section 24. Ca sulphate as fibers (left) and Ca-Na sulphate as plates (right)

7 Summary and discussion

A 50-cm long column of the sand/bentonite mixture used in the HE-E in situ test was heated on its base to 140°C while Pearson water was supplied through its upper surface at a very low pressure. The test was carried out in a Teflon cell equipped with relative humidity and temperature sensors. After almost three years of operation the cell was dismantled and the mixture analysed.

The test started by a heating phase (without hydration) which showed that the thermal conductivity of the dry materials is low, what caused a high difference in temperature between the heater surface and the sensor located at 10 cm, generating a high thermal gradient near the heater, and low temperatures in the rest of the column. A reason for this low temperature could be the bad thermal contact between the heater plate and the mixture, due to its low porosity and homogeneous grain size distribution. Another reason could be the heat

conduction and dissipation through the bottom of the cell, which could have taken place despite the isolation material. The stabilisation of the temperature was very quick though. The movement of water in the vapour phase as a result of the thermal gradient was evinced by the sharp increase of relative humidity recorded by the sensor closest to the heater –followed by a continuous decrease– and the slower increase recorded by the other two sensors. The high permeability of the mixture caused this process to be quite quick. When the heater was set to 100°C it took 120 h for the RH to reach a peak value of 70% at 10 cm from the heater (sensor 3), and when it was set to 140°C it took just 11 h for the RH to reach a peak value of 42% at the same location. The relative humidity increase in the upper part of the column when the heater was set to 100°C started just after about 20 h. Consequently, the relative humidity gradient at the end of the heating phase was sharp.

The water front moved forward along the column quite quickly. The arrival of the water front implied a sudden increase in temperature, which was consecutively recorded by sensor 1, 2 and then 3. Prior to this temperature rise there was a temperature decrease of about 10°C recorded by sensor 3 and a slight decrease recorded by sensor 2. The difference in thermal conductivity between the wet and the dry material could be responsible for this sudden decrease, because the thermal dissipation upwards (where the material was more saturated and had higher thermal conductivity) would be temporarily very large. Once the water front surpassed the sensors, the temperature increases took place. Three factors could have contributed to this temperature rise: the increase in thermal conductivity of the material with water content, the increase in thermal conductivity due to the improvement of the contacts among grains caused by the swelling of the bentonite and the hydration heat of the bentonite, that makes the hydration process to be exothermic. The energy released would be higher the lower the water content of the clay at the beginning of hydration, and consequently the temperature increase was higher towards the bottom of the column, where the material was drier. After 387 h the three sensors were flooded, i.e. indicated relative humidity values around 100% and afterwards failed recording relative humidity. Sensor 3 stopped working and became irreversibly damaged after 945 days of hydration, probably due to the harsh conditions imposed by the high temperature, humidity and salinity. An overall soft decrease of *T* after saturation was recorded over time, which could be attributed to the increase in thermal conductivity with water content.

The water intake rate was very large until the bottom sensor became flooded. Afterwards the pace softened and in fact it seemed to completely stop. This was due to the occurrence of gas bubbles that blocked the hydration system, since the injection pressure applied was very low and unable to dissolve them. To solve this, a purge system consisting of a syringe connected to the hydration line was implemented after 5183 h of hydration. After purging, the water intake resumed. Unfortunately, at some moment this purging system must have started to leak and from then on the water intake measurement was overestimated, by more than 200 g at the end of the test. The water intake measurement can be considered reliable until the installation of the purging system, when it was 659 g.

After 2.8 years of hydration the test was dismantled and it was observed that the column was completely and homogeneously saturated, except for the 2 cm closest to the heater, which were very dry. The high temperature in the area hindered its saturation, despite the high permeability of the mixture. In the rest of the column, the material had a cohesive consistence, an average degree of saturation of 93% and it was possible to subsample it. The pore size distribution analyses performed by MIP revealed also the homogeneity of the material along the column, since all the samples presented similar patterns, except those located closer to the heater. About 80% of the pores were larger than 50 nm, with a mode around 58 µm. With

respect to the original material this means that the number of macropores and its size decreased, whereas the number of smaller pores increased. This would be due to the swelling of the bentonite and filling of macro-voids upon saturation. Near the heater the pore size distribution was substantially different.

SEM observations revealed abundant chlorides and sulphates which came probably from the Pearson water used to saturate the mixture. The fact that these salts were also found at the bottom of the column could be an indication that the liquid water loaded with ions reached this area and evaporated again towards the cooler, upper areas, leaving precipitated salts. This would be an evidence of the formation of convective cells near the heater. The increase in salinity could affect the hydromechanical properties of the mixture.

8 References

ENRESA 2005. Ventilation experiment in Opalinus Clay for the management of radioactive waste. Publicación Técnica ENRESA 07/2005. Madrid, 82 pp.

Fernández, A.M. 2011. Determination of the Specific Heat Capacity of materials used as confinement barrier at El Cabril. Interim Report CIEMAT/DMA/2G208/3/11, 26 pp.

Gaus, I., Wieczorek, K., Mayor J.C., Trick T., García-Siñeriz, J.L., Schuster, K., Garitte, B., Kuhlman, U. 2011. EBS behaviour immediately after repository closure in a clay host rock: the HE-E experiment (Mont Terri URL). Proceedings of the 14th Int. Conference on Environmental Remediation and Radioactive Waste Management ICEM'11. September 25-29, 2011, Reims, France. P-59288. ASME, 7 pp.

Johnson, L.H., Niemeyer, M., Klubertanz, G., Siegel, P., Gribi, P. (2002): Calculations of the temperature evolution of a repository for spent fuel, vitrified high-level waste and intermediate level waste in Opalinus Clay. Nagra Technical Report NTB 01-04. Nagra, Wettingen, Switzerland.

Pearson F., 1998. Artificial waters for use in laboratory and field experiments with Opalinus Clay *Paul Scherrer Institut. TM 44-98-08*

Plötze M., Weber H.P (2007): ESDRED: Emplacement tests with granular bentonite MX-80: Laboratory results from ETH Zürich. Nagra Arbeitsbericht NAB 07-24. Nagra, Wettingen.

Sing, K.S.W., Everett, D.H., Haul, R.A.W., Moscou, L., Pierotti, R.A., Rouquérol, J., Siemieniewska, T. 1985. Reporting physisorption data for gas/solid systems with special reference to the determination of surface area and porosity. Pure & Appl. Chem. 57(4): 603-619. IUPAC.

Teodori, S.P., Gaus, I. (Eds.) 2011. Long Term Performance of Engineered Barrier Systems (PEBS). Mont Terri HE-E experiment: as built report. Nagra Arbeitsbericht NAB 11-25. Nagra, Wettingen, 125 pp.

Villar, M.V. 2013. Long-term THM tests reports: Isothermal infiltration tests with materials from the HE-E. PEBS Deliverable 2.2-7.2. CIEMAT Technical Report CIEMAT/DMA/2G210/07/2013. Madrid, 32 pp.

Villar, M.V.; Martín, P.L. & Barcala, J.M. 2005a. Infiltration tests at isothermal conditions and under thermal gradient. Informe Técnico CIEMAT/DMA/M2140/1/05. Madrid, 24 pp. Abril 2005.

Villar, M.V.; Martín, P.L. & Barcala, J.M. 2005b. Modification of physical, mechanical and hydraulic properties of bentonite by thermo-hydraulic gradients. Engineering Geology 81(3): 284-297.

Villar, M.V.; Sánchez, M. & Gens, A. 2008. Behaviour of a bentonite barrier in the laboratory: experimental results up to 8 years and numerical simulation. Physics and Chemistry of the Earth 33: S476-S485.

Villar, M.V.; Martín, P.L.; Gómez-Espina, R.; Romero, F.J. & Barcala, J.M. 2012. THM cells for the HE-E test: setup and first results. PEBS Deliverable 2.2-7.1. Technical Report CIEMAT/DMA/2G210/03/2012. Madrid, 34 pp.

Villar, M.V.; Martín, P.L. & Romero, F.J. 2014. Long-term THM tests reports: THM cells for the HE-E test: update of results until February 2014. PEBS Deliverable 2.2-7.3. Technical Report CIEMAT/DMA/2G210/03/2014. Madrid, 19 pp.

Appendix 1 VALUES RECORDED BY SENSORS

Table A- I: Relative humidity (RH) and temperature (T) recorded by sensors while the heater T was set to 100°C in cell S/B (sensor 1 placed at 40 cm from the bottom, sensor 2 at 22 cm and sensor 3 at 10 cm)

Time[a] (h)	Heater *T* (°C)	RH1 (%)	T1 (°C)	RH2 (%)	T2 (°C)	RH3 (%)	T3 (°C)
0	22	52	22.5	47	22.4	46	22.4
1	100	52	22.7	47	22.6	46	23.0
2	100	52	22.9	47	22.9	47	24.9
5	100	53	23.2	47	23.5	49	28.3
10	100	53	23.4	47	23.8	52	31.2
20	100	53	23.1	48	23.9	56	33.3
40	100	54	22.8	49	23.8	62	33.0
80	100	57	23.4	50	24.4	70	32.9
158	100	60	22.9	52	23.9	69	32.5
199	100	61	23.5	53	24.7	67	33.2
409	100	67	21.9	57	23.2	60	47.9
603	100	70	21.0	60	22.2	56	31.0
803	100	72	20.3	62	21.6	53	30.5
1303	100	74	20.2	65	21.4	48	30.3
1602	100	74	21.4	67	23.6	47	35.3
2001	100	74	20.3	73	23.8	40	39.5
2498	100	76	22.9	74	26.2	36	41.4

[a]Time since start of heating at 100°C

Table A- II: Relative humidity (RH) and temperature (T) recorded by sensors while the heater T was set to 140°C in cell S/B (sensor 1 placed at 40 cm from the bottom, sensor 2 at 22 cm and sensor 3 at 10 cm)

Time[a] (h)	Time[b] (h)	RH1 (%)	T1 (°C)	RH2 (%)	T2 (°C)	RH3 (%)	T3 (°C)
2499	1	76	23.0	74	26.3	36	41.5
2500	2	76	23.0	74	26.4	37	42.4
2503	5	76	23.1	74	26.6	41	46.5
2508	10	76	23.1	75	27.4	42	49.8
2518	20	76	23.6	76	28.6	42	51.5
2538	40	76	23.9	77	29.2	40	51.9
2580	82	76	24.2	78	29.3	37	51.9
2656	158	76	23.8	80	29.0	34	51.6

Time[a] (h)	Time[b] (h)	RH1 (%)	T1 (°C)	RH2 (%)	T2 (°C)	RH3 (%)	T3 (°C)
2700	202	76	22.7	80	28.0	33	50.8
2907	409	78	23.8	81	28.9	29	51.7
3103	605	78	22.0	80	27.1	27	50.4
3300	802	80	23.8	79	28.8	26	51.7
3692	1194	82	22.8	77	27.8	24	51.0

[a]Time since start of heating at 100°C; [b]Time since start of heating at 140°C

Table A- III: Relative humidity (RH) and temperature (*T*), water intake and laboratory *T* during the hydration phase, which started 3696 h after the beginning of heating in cell S/B (sensor 1 placed at 40 cm from the bottom, sensor 2 at 22 cm and sensor 3 at 10 cm)

Time[a] (h)	Lab *T* (°C)	Heater power (W)	RH1 (%)	T1 (°C)	RH2 (%)	T2 (°C)	RH3 (%)	T3 (°C)	Water intake (g)
0.0	19.8	10.6	82	22.8	77	27.8	24	51.0	37[b]
1.6		9.7	82	22.8	77	27.8	24	51.0	75
2.6		10.0	82	22.9	77	27.9	24	51.1	78
4.6	20.3	10.5	82	23.1	77	28.2	24	51.3	82
10	19.8	10.4	82	23.4	77	28.3	24	51.4	89
24	20.5	9.9	82	23.5	77	28.3	24	51.4	105
51	20.4	9.7	92	23.3	77	28.3	24	51.4	136
99	19.7	9.8	98	23.6	76	28.4	24	51.5	212
123	20.4	9.9	98	23.8	76	28.4	24	51.5	252
147	21.0	9.8	98	24.0	76	28.3	23	51.6	294
171	20.2	10.3	98	24.1	89	27.4	23	51.4	334
275	20.4	9.9	99	24.7	100	31.1	64	45.2	477
315	20.7	10.4	99	24.6	109	32.7	98	48.4	527
459	20.5	11.5	99	26.0	110	37.8	100	60.2	578
603	21.9	12.4	99	28.3	100	40.3	100	63.1	594
747	21.8	11.5	99	28.2	100	40.8		64.7	604
891	21.1	12.5	99	27.4	100	40.3		64.1	607
1063	21.8	13.0	99	28.2	100	42.3		68.0	632
1319	22.3	12.8	99	28.2		41.9		66.7	648
1851[c]	21.6	11.8	99	28.3		41.8		66.6	695
2572	21.9	11.8	99	29.0		42.3		66.7	717
3292	21.5	12.6	99	28.4		41.7		65.9	725
4012	19.7	11.9	99	26.8		40.3		64.7	733
4731	19.1	12.0	99	25.6		39.2		63.7	740
5451	18.5	12.3	99	24.8		38.3		62.7	747

Time[a] (h)	Lab *T* (°C)	Heater power (W)	RH1 (%)	T1 (°C)	RH2 (%)	T2 (°C)	RH3 (%)	T3 (°C)	Water intake (g)
6171	22.0	12.2	99	24.7		38.3		62.6	755
6892	18.7	12.9	98	25.1		38.6		62.8	762
7612	18.9	11.9	98	24.9		38.6		62.7	768
8332	21.1	12.6	98	27.2		40.5		64.2	773
9052	18.8	12.4	98	25.2		38.8		62.8	780
9772	20.7	11.7	98	27.1		40.2		63.9	786
10490	21.8	11.8	100	29.0		41.8		65.0	792
10802	22.7	11.9	99	29.3		41.9		65.0	793
11618	22.8	12.5	101	29.4		41.9		65.0	802
12603	21.3	11.7	99	28.4		41.0		64.0	798
13275	21.2	12.2	100	27.6		40.4		63.6	804
13994	18.5	12.0	99	25.0		38.3		62.0	811
14690	20.2	12.9	99	25.3		38.5		62.2	818
15506	19.5	12.9	99	25.3		38.5		62.2	824
16322	22.9	12.8	100	26.1		39.1		62.8	830
16946	19.1	12.2	98	25.4		38.7		62.4	835
17663	18.6	12.4	98	26.3		39.3		62.9	839
18386	20.5	12.0	99	26.2		39.3		62.7	844
19178	20.9	11.6	107	27.7		41.3			849
19850	19.6	11.7	106	28.5		42.5			853
20594	20.8	12.3	104	28.1		43.2			859
21386	20.7	11.8	105	27.2		42			865
22189	20.7	11.8	109	27		42.6			871
22885	21.4	13.3	110	27.2		42.4			876
23569	19.5	12.2	106	25.3		44.6			882
24289	19.8	11.6	105	25.2		43.6			886
24551	19.6	12.7	108	24.9		41.8			887

[a]Time since start of hydration; [b]Taken accidentally at the beginning of heating; [c]The water intake after this time is not reliable

Appendix 2 POSTMORTEM RESULTS

Table A- IV: Final measurements of dry density and water content

Section	Distance from surface (cm)	Water content (%)	Dry density (g/cm^3)	Degree of saturation (%)
1	1	27.8	1.46	89
2	3	29.8	1.44	91
3	5	33.2	1.40	96
4	7	31.0	1.42	92
5	9	30.3		
6	11	31.5		
7	13	30.6		
8	15	29.8	1.38	84
9	17	28.0		
10	19	28.5	1.48	92
11	21	29.9	1.42	89
12	23	28.6	1.45	89
13	25	28.5	1.46	90
14	27	28.9	1.45	90
15	29	30.9	1.43	94
16	31	33.2	1.41	97
17	33	33.4	1.41	98
18	35	34.7	1.34	92
19	37	29.9	1.44	92
20	39	30.3	1.46	97
21	41	31.5	1.46	99
22	43	32.5	1.42	97
23	45	28.1	1.50	94
24	47	4.2		
contact	49	2.7	1.69	12

Table A- V: Pore size distribution of samples taken along the column obtained by MIP

Section	Distance from hydration surface (cm)	Macropores (>50 nm), %	Mode macropores, µm	Mesopores (50-7 nm), %	Mode mesopores, nm	Micropores (<7 nm), %
1	1	84	48	6	14	10
2	3	83	39	5	15	13
3	5	76	59	4	12	19
4	7	75	48	4	12	21
5	9	82	59	4	14	14
6	11	77	66	3	21	20
7	13	92	90	8	19	0
8	15	93	73	7	11	0
9	17	82	26	4	15	13
10	19	91	32	5	17	3
11	21	80	39	6	23	14
12	23	86	43	5	15	9
13	25	90	39	6	15	5
14	27	85	81	6	23	9
15	29	75	43	5	11	20
16	31	94	73	5	11	1
17	33	79	48	5	15	16
18	35	78	39	5	15	17
19	37	82	110	5	17	13
20	39	87	81	6	21	6
21	41	81	53	5	17	13
22	43	76	59	4	14	20
23	45	78	81	6	15	15
24	47	49	99	8	19	43
contact	49	57	121	9	17	34